ABSTRACT

Synthesis of Vascular Disrupting Agent Payloads, Protease Specific Linkers, and their Corresponding Constructs

Abigail Brinson Smith

Director: Kevin G. Pinney, Ph.D.

The discovery and development of small-molecule anticancer agents that are both highly efficacious and selectively targeted remains a formidable goal and challenge. Conventional chemotherapy regimens often employ the use of cytotoxic agents which fail to differentiate between normal and cancerous tissue and are thus limited by their high degree of toxicity to normal tissue. Antibody-drug conjugates (ADCs) represent an emerging class of biopharmaceutical therapeutics that deliver highly potent anticancer agents (payloads) selectively to tumors or components of the tumor microenvironment. ADCs are comprised of a drug (payload) which is joined through an appropriate linker to an antibody or engineered protein. Pairing both a high degree of selectivity through the antibody with a high degree of cytotoxicity through the payload, ADCs represent an emerging and promising class of chemotherapeutic agents. Two small-molecule payloads (KGP05 and KGP18, previously discovered in the Pinney Laboratory) function as both highly potent antiproliferative agents (cytotoxins) and as highly effective vascular disrupting agents (VDAs). Details regarding the synthesis of these payloads and the preparation of drug-linker constructs tethering these payloads to the protease cleavable dipeptide linker Val-Cit-PABOH, widely used in ADC research, are presented.

APPROVED BY DIRECTOR OF HONORS THESIS:

Dr. Kevin G. Pinney, Department of Chemistry and Biochemistry

APPROVED BY THE HONORS PROGRAM:

Dr. Elizabeth Corey, Director

DATE: _____

SYNTHESIS OF VASCULAR DISRUPTING AGENT PAYLOADS, PROTEASE SPECIFIC LINKERS, AND THEIR CORRESPONDING CONSTRUCTS

A Thesis Submitted to the Faculty of

Baylor University

In Partial Fulfillment of the Requirement for the

Honors Program

By

Abigail Brinson Smith

Waco, Texas

May 2020

TABLE OF CONTENTS

ABBREVIATIONS

° C	Degree Celsius
Å	Angstrom
ABC	ATP-Binding Cassette Transporter
AcBut	4-(4-acetylphenoxy) butanoic acid
ACN	Acetonitrile
ADC	Antibody-Drug Conjugate
CA4	Combretastatin A-4
CA4P	Combretastatin A-4 Phosphate Salt
Cit	Citrulline
DIPEA	*N*, *N*-Diisopropylethylamine
DM1	*N*-2'-Deacetyl-N2'-(3-mercapto-1-oxopropyl) maytansine
DMF	*N*, *N*-Dimethylformamide
DNA	Deoxyribonucleic Acid
ESI	Electrospray ionization
h	Hour
HPLC	High Pressure Liquid Chromatography
Hz	Hertz
KOtBu	Potassium *tert*-butoxide
SEM	Scanning Electron Microscopy
mAb	Monoclonal Antibody
Mc	Maleimidocaproyl

MCC	4-[*N*-maleimidomethyl] cyclohexane-1-carboxylate
MDR	Multi-drug resistance
MHz	Megahertz
min	Minutes
mM	Millimole
MMAE	Monomethyl Auristatin E
NMR	Nuclear Magnetic Resonance Spectroscopy
OSu	*O*-Succinimide
PABOH	*Para*-aminobenzyl alcohol
PEG4Mal	4-arm Polyethylene glycol-maleimide
PNP	*P*-Nitrophenol
SEM	Scanning Electron Microscopy
SMCC	Succinimidyl 4-(*N*-maleimidomethyl) cyclohexane-1-carboxylate
SPDB	*N*-succinimidyl-4-(2-pyridyldithio) butanoate
THF	Tetrahydrofuran
Val	Valine
VDA	Vascular Disrupting Agent

ACKNOWLEDGMENTS

This research project would not have been possible without the support of many people.

It is with immense gratitude that I acknowledge the support and help of Dr. Kevin G.

Pinney and Jacob W. Ford.

DEDICATION

Honors thesis by Abigail Brinson Smith, dedicated

To,

My Loving Family,

Supportive Friends,

and

Encouraging Mentors

CHAPTER ONE

Background

Cancer and Nature of Vasculature in Tumors

The National Cancer Institute defines cancer as a collection of related diseases that are connected by the general characteristic of a sub-set of cells that begin to continuously divide and spread into surrounding tissues.[1] This is driven by mutations within a cell's DNA, prohibiting the natural growth and division checkpoints from being observed, leading to uncontrolled growth.[1, 2] This continuous division within a specific tissue eventually leads to the formation of a tumor from which malignant cells can break off of and invade other healthy tissues and form new growths around the body in an event known as metastasis.[1] Without early detection and treatment, cancer can lead to severe health consequences, including death. Various methods have been sought to cure this disease including radiation, surgery, and chemotherapeutic drugs – the latter of the three being the focus of this thesis.[2] These drugs serve to kill malignant cells; however, major problems with these drugs are specificity and cytotoxicity to cancer cells rather than healthy cells.[2] Within anti-cancer biopharmaceutical drug research field is a branch that focuses on targeting the tumor's blood supply, or vasculature, as it embodies unique and targetable characteristics within a tumor.[2]

In healthy tissue, cells are provided nutrients through a complex and well-organized system of blood vessels and vasculature that deliver key metabolic components to tissue beds.[3] These systems of vessels are maintained by pro-angiogenic processes and anti-angiogenic processes that balance each other out in order to meet the demands of the

tissue.[3] This process of developing new vessels from pre-existing ones is known as angiogenesis.[3] However, once a cell becomes cancerous and begins the process of rapid division, it must quickly recruit additional vasculature to deliver more nutrients to meet the demands of the highly metabolic cancerous cells.[3] The balance between pro-angiogenic and anti-angiogenic processes becomes severely skewed towards pro-angiogenesis without being deterred by the normal checkpoints.[3] In doing so, the previously well-organized network of blood vessels is forced to haphazardly branch, forming a weak, brittle knot of vasculature within the developing tumor.[3] The rapid rate at which these vessels grow contributes to their brittle nature, thus creating a distinct target for cancer therapeutic drugs.[4] The most effective and correspondingly safest cancer therapeutic agents are able to target cancer cells while limiting deleterious effects to healthy cells.[4]

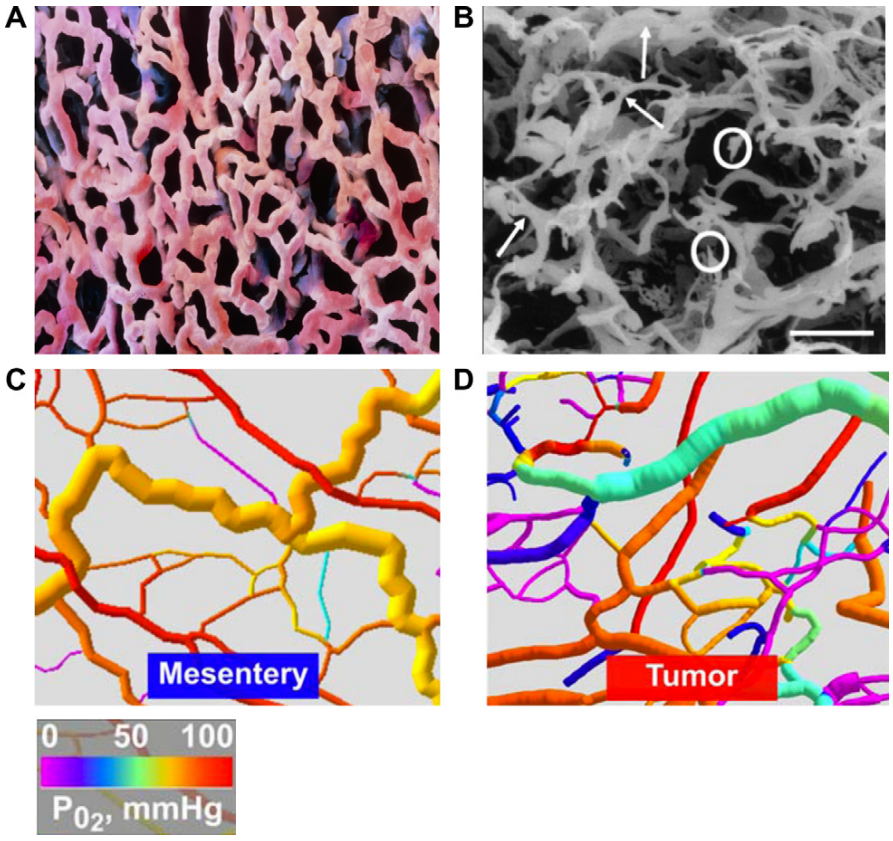

Figure 1: Panel A depicts a Scanning Electron Microscopy (SEM) of normal lung tissue. Panel B depicts an SEM of a human sigmoidal adenocarcinoma. The contrast between these two images reveals the obvious unorganized nature of tumor vasculature in comparison to that of normal tissue. Panels C and D display the differences in organization and distribution of PO_2 of normal and cancerous tissue. These differences offer an ability for partial selectivity of therapeutic drugs.[3] Reprinted from *Cancer Treatment Reviews*, Vol. 37, Dietmar W. Siemann, The unique characteristics of tumor vasculature and preclinical evidence for its selective disruption by Tumor-Vascular Disrupting Agents, Page No. 64, Copyright (2011), with permission from Elsevier.

Targeting the vascular network in cancer treatments comes in two forms.[3] On one hand, drugs can target the process of the development of new vessel networks, otherwise known as the anti-angiogenic approach.[4] Alternatively, drugs can target the already developed, but compromised blood vessel network in tumors, known as the anti-vasculature approach.[4] These two approaches have also been used in conjunction with one another; the anti-angiogenesis drugs can prevent the tumor from growing larger and the anti-vasculature drugs can cut of blood supply to the interior of the tumor.[4] In theory, together, these drugs can kill a tumor by starving it of the nutrients and oxygen it so heavily relies on.[4] These unique microenvironment features allow for drugs to be developed that target these specific endothelial cells in tumors and lead to massive tissue necrosis.[4]

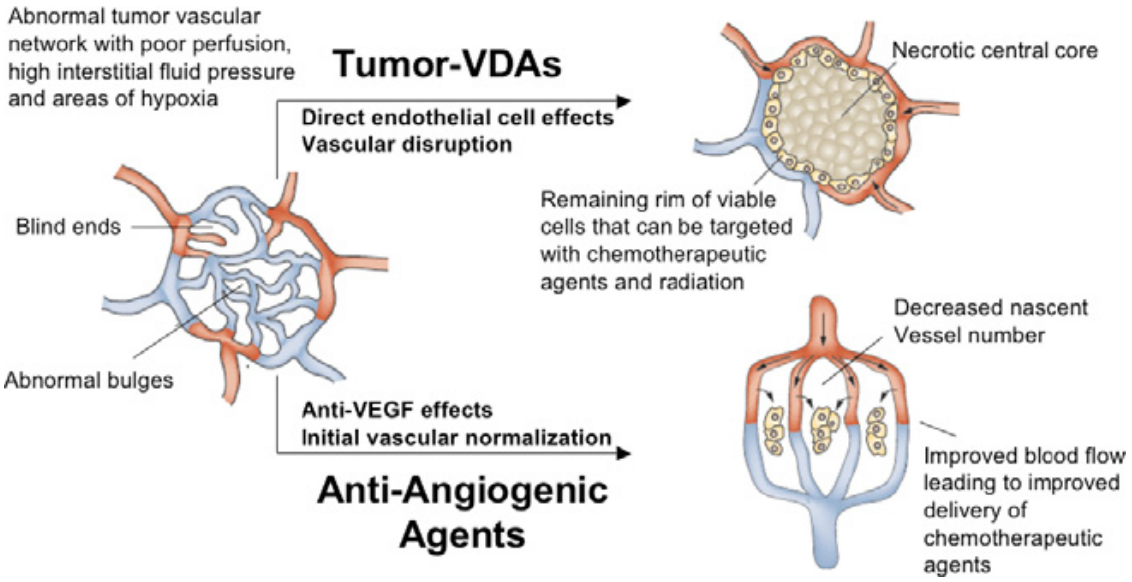

Figure 2: Diagram displaying the two different approaches to targeting tumor vasculature.[3] Reprinted from *Cancer Treatment Reviews*, Vol. 37, Dietmar W. Siemann, The unique characteristics of tumor vasculature and preclinical evidence for its selective disruption by Tumor-Vascular Disrupting Agents, Page No. 65, Copyright (2011), with permission from Elsevier.

Natural Products and Tubulin Inhibition

The biological effects associated with inhibition of tubulin polymerization include both antiproliferative (cytotoxic) behavior as well as destruction of tumor-associated vasculature mediated by morphology (shape) changes in the long, thin endothelial cells causing them to become round, thereby affecting the integrity of the blood vessel walls by introducing leaky holes in the vessel network.[3] This subsequently, leads to reduced red blood cell flow which leads to red blood cell stacking which leads to high blood viscosity.[3] All of these factors result in the insufficient delivery of nutrients to the core of the tumor.[3] Once the nutrient supply has been cut off to the center of the growth, tumor necrosis ensues.[3]

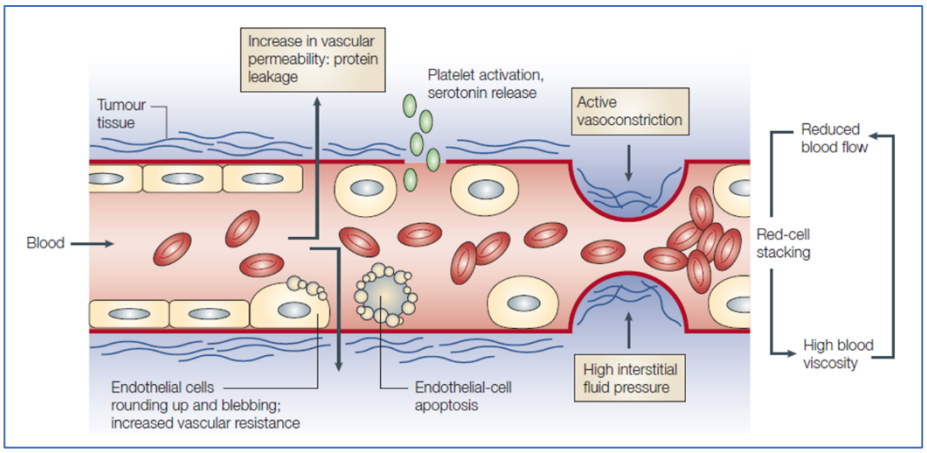

Figure 3: This image depicts the effects of vascular disruption.[5] Reprinted by permission from Springer Nature: *Nature Reviews Cancer*, Disrupting tumour blood vessels, Gillian M. Tozer et al, Copyright (2005).

In order to induce this conformational change, it was discovered that the natural product, colchicine was a strong inhibitor of tubulin polymerization and was initially investigated for potential use in cancer therapies. However, the use of colchicine had undesired effects that ultimately diminished its utility as a chemotherapeutic agent; however, hope remained as the colchicine binding site on tubulin could still be targeted through synthesis of colchicine derivatives and analogues. Some adverse effects of colchicine include gastrointestinal irritation at low doses, while at higher doses more serious implications such as hepatocellular damage, CNS toxicity, respiratory depression, and cardiovascular collapse may occur making it too dangerous to be seriously considered as a chemotherapeutic.[6] However, in smaller doses colchicine is currently approved to medically treat acute gout and recurrent pericarditis.[6]

The discovery and development of new small-molecule inhibitors of tubulin polymerization that interact at the colchicine binding site offers the potential promise for

improved therapeutic efficacy and selectivity while minimizing the unintended side-effects inherent to colchicine.[6] The natural products combretastatin A-1 (CA1) and combretastatin A-4 (CA4) were isolated from the African bush-willow tree, Combretum caffrum, by Pettit and co-workers.[7] These molecules where discovered to be potent inhibitors of tubulin polymerization, like colchicine, but with potentially fewer and less serious adverse effects, thus offering better promise as chemotherapeutic agents in comparison to colchicine (Figure 6).[7] From structure activity relationship (SAR) studies of the combretastatins, it was found that optimum inhibition of tubulin polymerization occurred when the following features were present: (1) the *cis* (*Z*) geometry about the alkene bridge, (2) the 4-5 Å distance between the aryl moieties, and (3) the trimethoxy phenyl group.[8] The payloads synthesized by The Pinney Group, KGP05 and KGP18, contain these three important structural features (Figure 4).[9-15] These VDAs bind to the colchicine binding site on the β-tubulin subunit of the αβ-tubulin heterodimer leading to tubulin inhibition and ultimately the disassociation of the endothelial cells lining the microvessels associated with the tumor leading to internal tumor necrosis.[3,11,12] The Pinney Group has found high degrees of cytotoxicity against cancer cell lines in their design and development of structurally diverse benzosuberene-based molecules along with corresponding analogues and derivatives.[12–15]

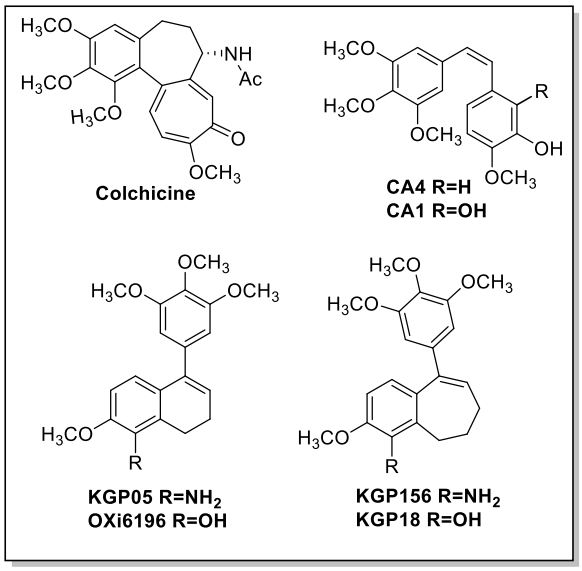

Figure 4: This image depicts the similarities between the tubulin inhibitors colchicine, CA1, CA4, and the synthetic payloads KGP05, KGP18, KGP156, and OXi6196.

The drug-linker constructs described in this thesis are intended to offer a high degree of selectivity for the tumor endothelial cells and a high degree of cytotoxicity through tubulin inhibition. Building on previous synthetic protocols established by the Pinney Group, the synthesis of these small-molecule therapeutic agents was modified to enhance overall yield and decrease production of undesired side products.[12,13,16,17] The linker Mc-Val-Cit-PABOH was synthesized and subsequently covalently tethered to the tubulin polymerization inhibitor, KGP05, and the resultant drug-linker construct is currently undergoing biological evaluation for its potential utility as a component in various ADCs and related conjugates.[18]

Antibody-Drug Conjugates and Payloads

ADCs consist of three basic components: the monoclonal antibody, the linker, and the drug payload. [18-21] Each piece of the ADC brings about an advantage to the overall compound in either increasing its selectivity or its cytotoxicity.[7]

VDAs are highly cytotoxic, but alone are only effective if they can impart selectivity to the endothelial cells lining the microvessels feeding tumors.[18] Thus, it is important when constructing an ADC to evaluate whether the mechanism of drug release is selective to conditions unique to the target cell or tumor microenvironment.[18] The tumor vasculature can be targeted through direct apoptotic effects or by inhibiting tubulin polymerization in order to alter endothelial cell shape and consequently preventing the vessel network from delivering nutrients and oxygen throughout the tumor.[3] In other words, disrupting the endothelial cell's shape, will impart severe consequences on its capacity to carry out its intended function.[3] The drugs discussed herein have been synthesized with the intention of altering the tubulin polymerization of tumor endothelial cells and have shown to be successful in this way.[9, 10] The payloads KGP05 and KGP18 both inhibit the ability of tubulin to function properly.[9, 10] This benzosuberene analog (KGP18) and dihydronaphthalene analog (KGP05) have been shown in biological studies to possess strong cytotoxicity (low nM to pM range) due to their ability to inhibit tubulin polymerization in human cancer cell lines.[22]

A major obstacle faced in the past with VDAs is multidrug resistance (MDR) facilitated by ATP-binding cassette (ABC) transporters in the cell membrane which function to pump out any foreign material present in the cell, severely decreasing the potency and efficiency of these VDAs; however, to circumvent this issue, there have been

studies looking into inhibiting these ABC transporters to further increase a drug's intracellular effect.[23] Moving forward, when testing the cytotoxicity of the VDAs synthesized herein, it would be interesting to compare their effect alone versus in the presence of an ABC transporter inhibitor. This problem was faced with the FDA approved, Mylotarg™, and is discussed in greater detail later on.

Another major obstacle with tumor VDAs, is the problem of the viable rim.[5] The tumor cells on the outer edge of the solid mass are able to remain viable despite the necrosis of the internal aspect of the tumor (Figure 5).[5] The periphery is less sensitive to vascular disruption which has been contributed to cells ability to extract nutrients and oxygen from the surrounding tissues.[5] However, studies have shown the problem is more complex revealing that the vasculature itself at the rim of the tumor is less affected than at the center.[5] This could be explained by the differences in interstitial pressure and the vascular architecture.[5] Interstitial pressure steadily rises moving from the rim to the center of a tumor and as a result, tumor microvessel permeability increases and becomes susceptible to losing vascular integrity.[5, 24] Further, with respect to the architecture, there are more small caliber vessels present at the center than at the rim of the tumor, which display a much higher sensitivity to the increase in interstitial pressure than the larger vessels present at the rim.[5, 25] This problem is circumvented by pairing VDA drugs with antibodies as the tumor periphery is the only tumor region that is easily accessible by high-molecular-weight therapeutics such as antibodies, making the combination of VDAs with these new approaches very attractive with ADC therapeutics.[5, 26]

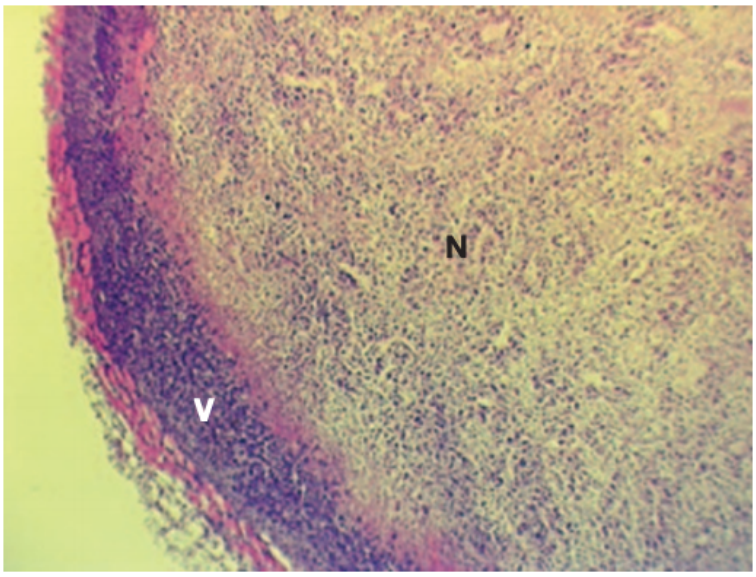

Figure 5: This image depicts the viable (V) cells at the rim of a tumor versus the necrotic (N) cells at the center of the tumor in a hematoxylin and eosin staining of paraffin embedded tissue of a mouse mammary carcinoma.[5] Reprinted by permission from Springer Nature: *Nature Reviews Cancer*, Disrupting tumour blood vessels, Gillian M. Tozer et al, Copyright (2005).

Additionally, proper function of the ADCs relies on a stable linker.[20] The linker is structurally responsible for the connection between the antibody and payload and functionally responsible for directing the subsequent release of the payload once the compound has reached the targeted site through either lysosomal processing of the antibody or a cleavable linker.[3,20] Its specific purpose is to keep the VDA drug (payload) in connection to the monoclonal antibody in order to minimize or prevent non-specific release.[18] There are cleavable linkers and there are non-cleavable linkers – this classification is assigned based on the mechanism of drug release (Figure 6).[18] Non-cleavable linkers rely on lysosomal degradation in order for drug release to occur, while cleavable linkers are sensitive to subtle changes in physiological conditions that can result in the release of the drug.[18] Further, cleavable linkers can be classified as either chemically labile or enzymatically labile.[18] Chemically labile linkers can be cleaved in acidic

environments or by an abundance of glutathione which reduces disulfide based linkers, while enzymatically labile linkers are cleaved by proteases that are highly expressed in cancer cells.[18] The linker synthesized herein was designed for selective proteolytic cleavage by cathepsin B.[4,18,30]

The first FDA approved ADC was Mylotarg® in 2000 that utilizes a non-peptide based linker; it was withdrawn from the market due to clinical failures, but has since been re-approved.[21,27] Mylotarg® clinical testing was expedited by the FDA and granted accelerated approval for patients with acute myeloid leukemia (AML) aged 60 years and older who were not eligible for cytotoxic chemotherapy.[28] Once more testing was complete, it was observed that as a result of Mylotarg®, patients suffered severe hepatotoxicity in the form of sinusoidal obstructive syndrome (SOS) or hepatic veno-occlusive disease (VOD); Mylotarg® offered no survival benefit in comparison to standard chemotherapeutic treatments and was complicated by severe adverse effects, prompting its subsequent removal from the market.[28] One proposed reason for this was that the cancer cells exhibited an overabundance P-glycoprotein (a type of ABC transporter) expressed in tumor cells which mediated drug-resistance. This is due to the fact that when the conjugate is processed intracellularly, hydrophobic cytotoxic metabolites are generated which are prime substrates for P-glycoprotein and are subsequently pumped out of the target cell.[28] In order to circumvent this issue of cell-mediated drug resistance, Kovtun and colleagues have described a maleimidyl-based hydrophilic linker, PEG4Mal (Figure 6), that appears to be a poor substrate for P-glycoprotein, thereby enabling the cytotoxic drug to remain inside the cell.[28,29] Enabling the cytotoxic drug to remain inside the cell has a double benefit as it enables the drug to impart its cytotoxic effects intracellularly, and it reduces the

severity of adverse effects as the amount of free circulating drug is minimized.[28] Since its removal from the market, Mylotarg® has been reapproved by the FDA as it was observed that Mylotarg® showed significantly less adverse effects for patients with acute promyelocytic leukemia (APL), a subtype of AML, due to the significantly lower presence of P-glycoprotein in these cancer cells.[28]

Especially prevalent is the cathepsin B cleavable Mc-Val-Cit-PABOH linker utilized in many pre-clinical ADC candidates, as well as the FDA approved ADC Adcetris® (brentuximab vedotin) in 2011.[21] An alternative route for the synthesis of the cathepsin B cleavable Mc-Val-Cit-PABOH linker is reported herein that involved six steps from *l*-Citrulline.[18] Importantly, this route avoided undesirable epimerization and proceeded with improved overall yield. Utilizing this methodology, a drug-linker construct incorporating a potent small-molecule inhibitor of tubulin polymerization (referred to as KGP05), was synthesized as a representative example. This linker was designed to be a cathepsin B cleavable dipeptide moiety for lysosomal release of the attached prodrug; however, biological studies suggest that it can also be cleaved extracellularly.[18,30,31] For example, it was observed that antigens such as CD20, CD21, CD22, which are known to be poorly internalized worked well in mouse cancer models with an anti-lymphoma ADC products.[32,33] This indicates that the ADC can maintain its cytotoxic effects even when the payload is unleashed outside of the cell. Because of this, using antibodies specific to fibrin or to collagen IV (extracellular matrix components) have been proposed as an attractive tumor targeting strategy known as the Cancer stromal targeting (CAST) approach.[32,34,35] It has been frequently observed in solid tumors that the blood coagulates at a higher than normal frequency which then subsequently creates a targetable fibrin deposition.[32,34,35]

This is important because *in vivo* studies have shown that antibodies have a slow rate of diffusion to the center of a solid tumor; however, if ADCs can target features of the outer rim tumor extracellular space and release their drug payloads here, they can diffuse and subsequently internalize into the innermost tumor cells, endothelial cells and in tumor-resident leukocytes at a faster rate.[32,34,35]

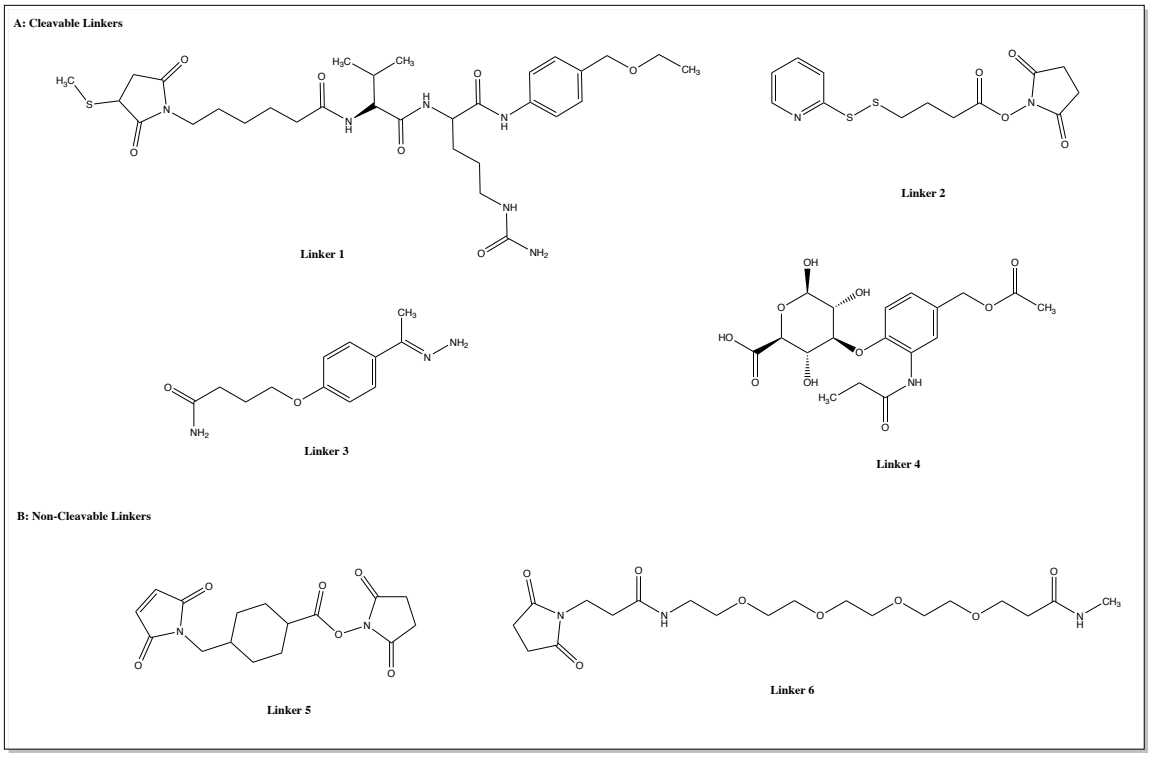

Figure 6: This image displays the wide variety and diversity in linker structures that can be used in ADCs. Panel A presents cleavable linkers: Linker 1 is a lysosomal protease sensitive Val-Cit dipeptide linker; Linker 2 is a Glutathione sensitive SPDB linker; Linker 3 is an acid sensitive AcBut linker; and Linker 4 is a β-Glucuronidase sensitive linker. Panel B presents non-cleavable linkers: Linker 5 is a SMCC linker; and Linker 6 is a PEG4Mal linker.[36]

Finally, the major source of drug specificity arises from the practice of tethering a monoclonal antibody (mAb) to the linker in order to deliver the highly cytotoxic payload with a high degree of specificity to antigens that are over-expressed in cancer cells.[20]

Determining which mAb will provide the highest degree of specificity is a whole area of research in itself.[37] The resulting physiological and morphological differences in tumors give rise to the expression of certain types of antigens that wouldn't normally be available for targeting.[37] It is complicated by the fact that every cancer is different, and every cancer presents different types of antigens on its surface and in different concentrations.[37] For example, even within the realm of breast cancer there are many different antigens that could be expressed depending on the specific type of cancer; specifically the ADC, Kadcyla™, targets the antigen HER2 which is often overexpressed in breast cancer.[3, 38]

The overall mechanism of the ADC begins when the antibody attaches to the specific antigen expressed on the surface of the cancerous cell.[20] This can be followed either by receptor mediated endocytosis or extracellular release of the payload into the tumor microenvironment (Figure 7).[3,20] The mechanism of action depends on the antigen targeted and the type of linker constructed.[20] The proteolytic cleavage can occur on the surface of the cells after the antibody attaches to the antigen, or it can occur within the cell during lysosomal degradation.[4,20]

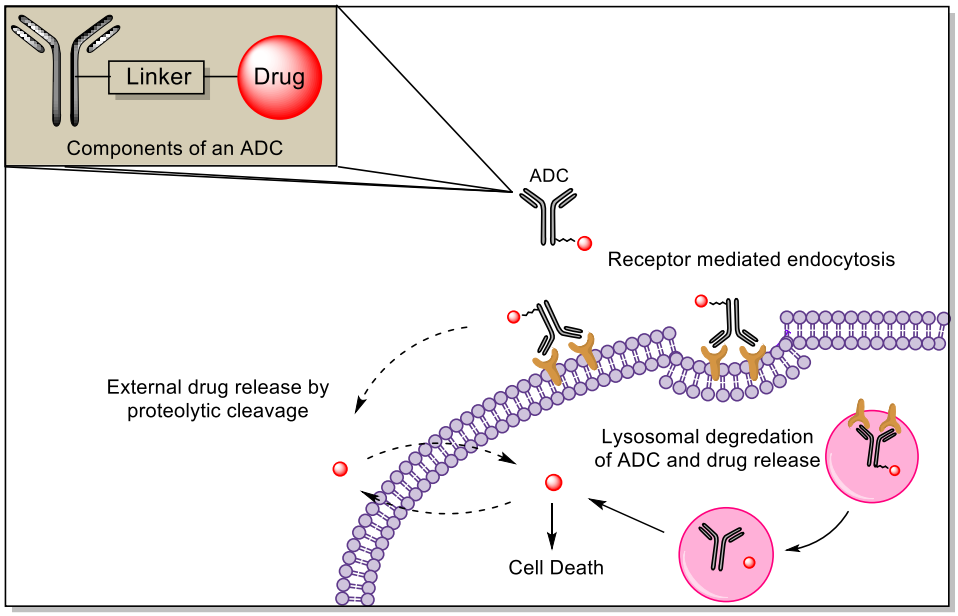

Figure 7: The image depicts the ADC mechanism of action in the delivery of a payload to a target cell.

Currently, the FDA has approved seven ADCs, two of which employ small-molecule inhibitors of tubulin polymerization as their payloads.[37,39] The seven that are currently approved include: Ado-trastuzumab emtansine (Kadcyla™), Brentuximab vedotin (Adcetris™), Inotuzumab ozogamicin (Besponsa™), Gemtuzumab ozogamicin (Mylotarg™), Polatuzumab vedotin-piiq (Polivy™), Enfortumab vedotin (Padcev™), and Trastuzumab deruxtecan (Enhertu™).[39] Three of the seven FDA approved ADCs, Brentuximab vedotin (Adcetris™), Polatuzumab vedotin-piiq (Polivy™), and Enfortumab vedotin (Padcev™), have similar chemical structures and all target microtubule polymerization through a Val-Cit Cathepsin B cleavable linker and MMAE payload tethered to a different antibody (mAb) based on type of cancer cell targeted.[40,41] Inotuzumab ozogamicin (Besponsa™) and Gemtuzumab ozogamicin (Mylotarg™) both feature payloads that function to cause double stranded breaks in DNA in target cells.[42,43]

Finally, Trastuzumab deruxtecan (Enhertu™) which features a payload that functions as a topoisomerase I inhibitor.[44]

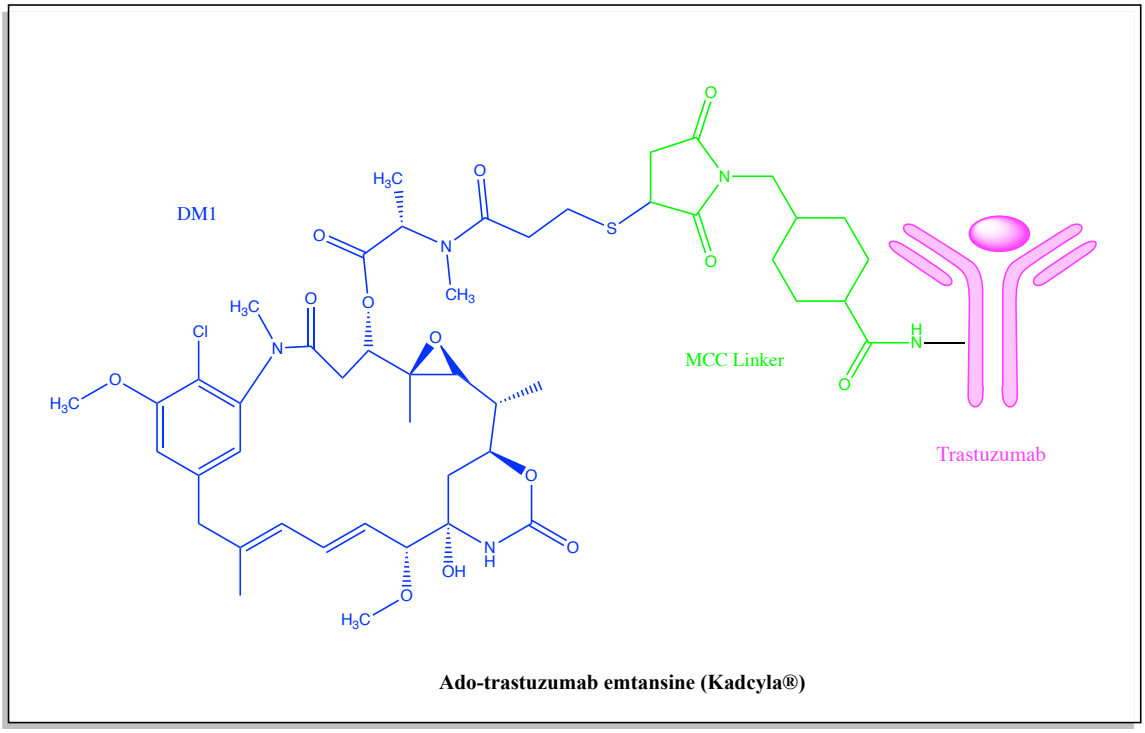

Figure 8: Depicted is the structure of the FDA approved ADC, Ado-trastuzumab emtansine (Kadcyla™) featuring a Tratuzumab antibody, MCC linker, and the DM1 payload which serves to inhibit tubulin polyermization.[45]

The four that employ small-molecule inhibitors of tubulin polymerization as their payloads are Brentuximab vedotin (Adcetris®) for Hodgkin's and anaplastic large cell lymphomas (Figure 9), ado-trastuzumab emtansine (Kadcyla®) for the treatment of HER2-positive breast cancer (Figure 8), Enfortumab vedotin (Padcev™) for urothelial cancer, and Polatuzumab vedotin-piiq (Polivy™) for relapsed or refractory diffuse large B-cell lymphoma.[37] The drug, Adcetris® tethers a mAb targeting CD30 antigens to a cathepsin B protease cleavable linker which is then attached to a mono-methyl auristatin E (MMAE) payload (Figure 9).[46] Adcetris® is a strong model for future drugs because the linker that

is employed in this drug is the dipeptide, Valine-Citrulline, which is selectively cleaved by the protease cathepsin B.[46] Cathepsin B is a good target due to its high abundancy specifically in the tumor microenvironment.[46] Once cleavage has occurred by cathepsin B, the spacer (*para*-amino benzyl alcohol moiety) then releases the payload at the targeted site through an elimination reaction.[46] The spacer is a moiety that is self-immolative and undergoes a spontaneous 1,6-elimination resulting in release of the prodrug payload within the cell.[18,47] There have been many studies conducted on the Mc-Val-Cit-PABOH linker in the ADC model of drug delivery; however, the work reported herein is novel in that it attaches unique and highly potent small-molecule VDAs to this promising linker.

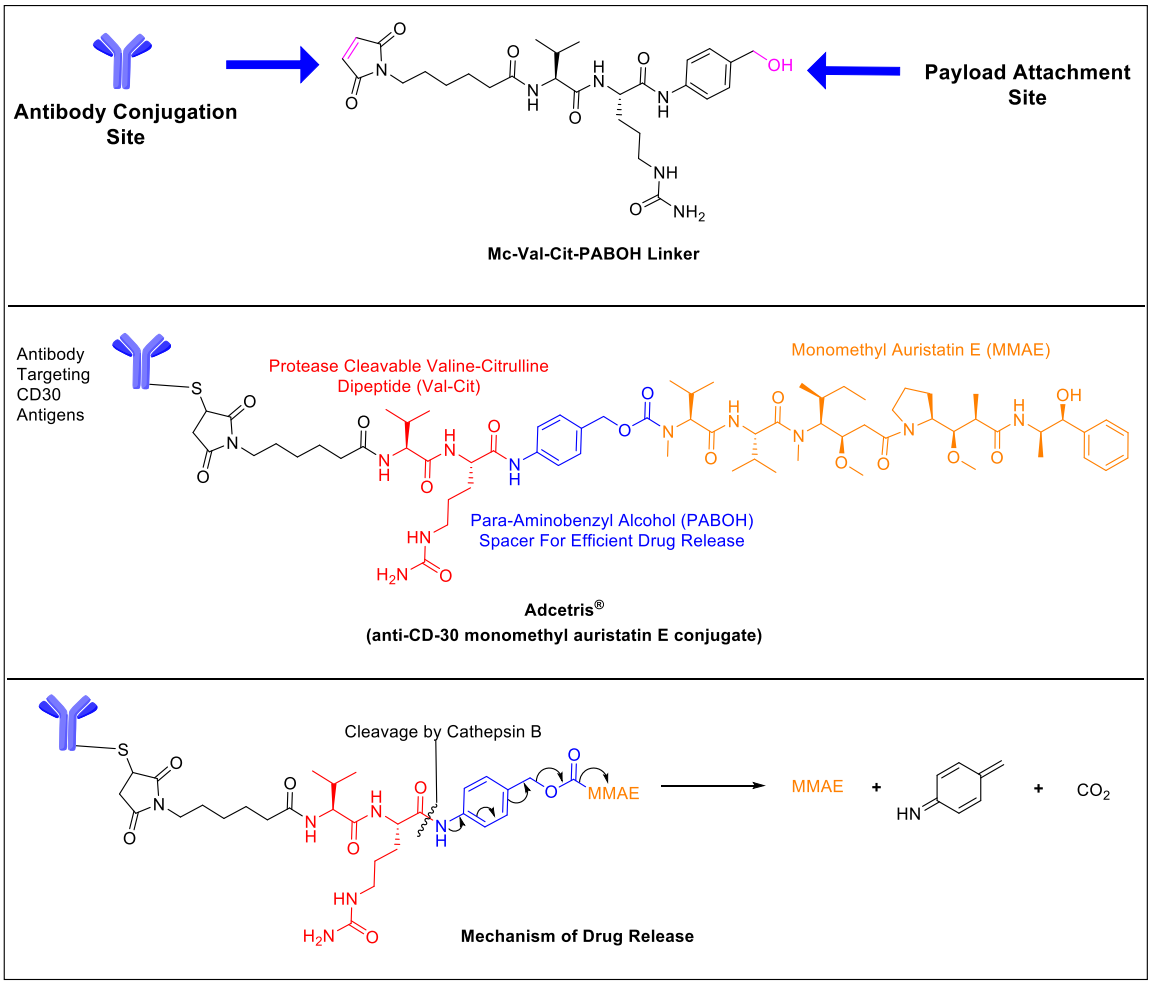

Figure 9: Adcetris® mechanism of drug release.

CHAPTER TWO

Materials and Methods

General Information

Tetrahydrofuran (THF), dichloromethane (DCM), dimethylformamide (DMF), and methanol (MeOH) were used in anhydrous forms. All of the reactions were carried out under an atmosphere of nitrogen in oven-dried glassware with magnetic stirring unless otherwise specified. Analytical thin layer chromatography was performed on 0.25 mm thick, silica gel 60-F254 plates. Visualization was accomplished with UV light or aqueous potassium permanganate solution staining followed by air heating. Purification of reaction products was carried out on a Biotage Isolera flash purification system using silica gel (200-400 mesh, 60Å).

^{1}H NMR spectroscopic data were recorded on a Bruker Ascend 600 (600 MHz) spectrometer and are reported in ppm using solvent as internal standard (e.g. DMSO-d6 at 2.50 ppm). Data are reported as: b = broad, s = singlet, d = doublet, t = triplet, q = quartet, p = pentet, m = multiplet; coupling constant(s) are expressed in Hz. ^{13}C NMR spectroscopic data were recorded on a Bruker Ascend 600 (150 MHz) spectrometer. Chemical shifts are reported in ppm with solvent resonance employed as the internal standard (e.g. DMSO-d6 at 39.5 ppm). High-resolution mass spectra were obtained under positive ESI using a Thermo Scientific LTQ Orbitrap. All the reagents were purchased from common suppliers.

HPLC data were recorded on an Agilent 1200 HPLC system with a diode-array detector (λ = 190-400 nm), a Zorbax XDB-C18 HPLC column (4.6 mm x 150 mm, 5 µm), and a Zorbax reliance cartridge guard column and are reported in percent purity. The

method used to obtain this data was through a 30-90 ACN gradient with a flowrate of 1mL per minute (Table 1).

30-90 ACN	Percent Water	Percent ACN
0 min	70	30
25 min	10	90
30 min	10	90

Table 1: 30-90 ACN method used in obtaining HPLC data.

Synthesis of Mc-Val-Cit-PABOH Linker

Synthesis of Fmoc-Citrulline (**Compound 1**)[18]

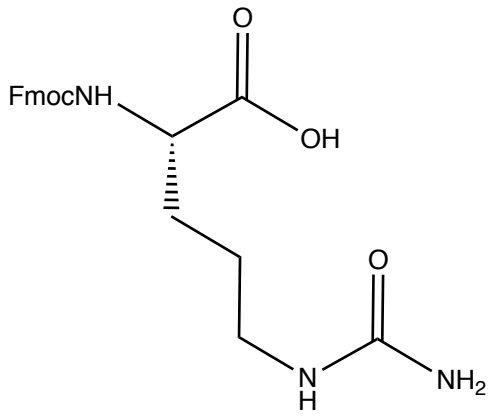

A solution of *l*-citrulline (1.500 g, 8.562 mmol, 1.100 eq) in water (0.2 M) was treated with sodium bicarbonate (1.439 g, 17.13 mmol, 2.201 eq). In a separate container, a solution of Fmoc-Cl (2.013 g, 7.784 mmol, 1.000 eq) in THF (0.2 M) was prepared. Following stirring for 30 minutes at room temperature, the Fmoc-Cl solution was added to the reaction. The reaction was allowed to stir for 24 hours at room temperature before removing the THF under reduced pressure. The aqueous layer was extracted (3X) with ethyl acetate and the organic layer was discarded. The aqueous layer was then treated with HCl (2 M) until a white precipitate was observed. The organic layer was then extracted (3X) following the addition of iPrOH [10 % by volume] – EtOAc. The organic phase was dried over sodium sulfate. The solvent was removed under reduced pressure. The remaining white solid was then sonicated and triturated with diethyl ether, which was then decanted off. This step was repeated twice to obtain a white solid which was dried under reduced pressure to obtain an analytically pure sample of Fmoc-Cit (3.165 g, 7.963 mmol, 93% yield). No further purification was required. ^{1}H NMR (600 MHz, DMSO-d_6) δ 12.56

(s, 1H), 7.89 (d, J = 7.6 Hz, 2H), 7.73 (d, J = 7.5 Hz, 2H), 7.67 (d, J = 8.0 Hz, 1H), 7.42 (t, J = 7.5 Hz, 2H), 7.38 – 7.28 (m, 2H), 5.94 (brs, J = 5.7 Hz, 1H), 5.38 (brs, 2H), 4.31 – 4.26 (m, 2H), 4.23 (q, J = 8.0, 7.4 Hz, 1H), 3.93 (m, J = 9.5, 8.0, 4.7 Hz, 1H), 2.95 (brt, J = 6.6 Hz, 2H), 1.70 (m, 1H), 1.57 (m, J = 14.1, 9.8, 5.0 Hz, 1H), 1.49 – 1.32 (m, 2H), 1.03 (d, J = 6.1 Hz, 1H).

Synthesis of Fmoc-Cit-PABOH (**Compound 2**)[18]

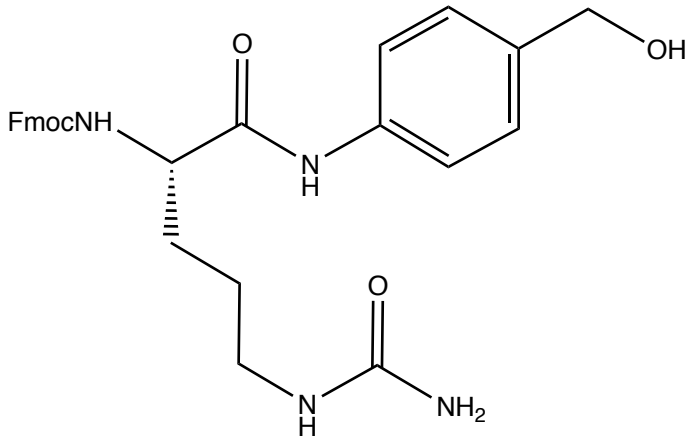

A solution of Fmoc-Citrulline (1.037 g, 2.620 mmol, 1.000 eq) and 4-aminobenzyl alcohol (0.964 g, 7.86 mmol, 3.00 eq) in DMF (0.2 M) was treated with DIPEA (0.456 mL, 2.62 mmol, 1.00 eq). Following stirring at room temperature for 15 minutes, HATU was added to the reaction. The solution was stirred for 48 hours in the dark at room temperature. DMF was removed under reduced pressure and the crude product was purified by flash column chromatography using 2-10% MeOH-DCM as solvent. Product was isolated as a white solid. (0.443 g, 0.882 mmol, 39% yield). ^{1}H NMR (500 MHz, DMSO-d_6) δ 9.99 (s, 1H), 7.89 (d, J = 7.6 Hz, 2H), 7.75 (t, J = 6.5 Hz, 2H), 7.68 (d, J = 8.0 Hz, 1H), 7.56 (d, J = 8.2 Hz, 2H), 7.44 – 7.38 (m, 2H), 7.36 – 7.28 (m, 2H), 7.24 (d, J = 8.2 Hz, 2H), 6.00 (brt,

J = 6.0 Hz, 1H), 5.43 (s, 2H), 5.10 (t, J = 5.7 Hz, 1H), 4.43 (d, J = 5.8 Hz, 2H), 4.29 – 4.12 (m, 4H), 3.07 – 2.99 (m, 1H), 2.98 – 2.89 (m, 1H), 1.72 – 1.63 (m, 2H), 1.62 – 1.54 (m, 2H), 1.50 – 1.42 (m, 1H), 1.42 – 1.33 (m, 1H).

Synthesis of Fmoc-Val-Cit-PABOH (**Compound 3**)[18]

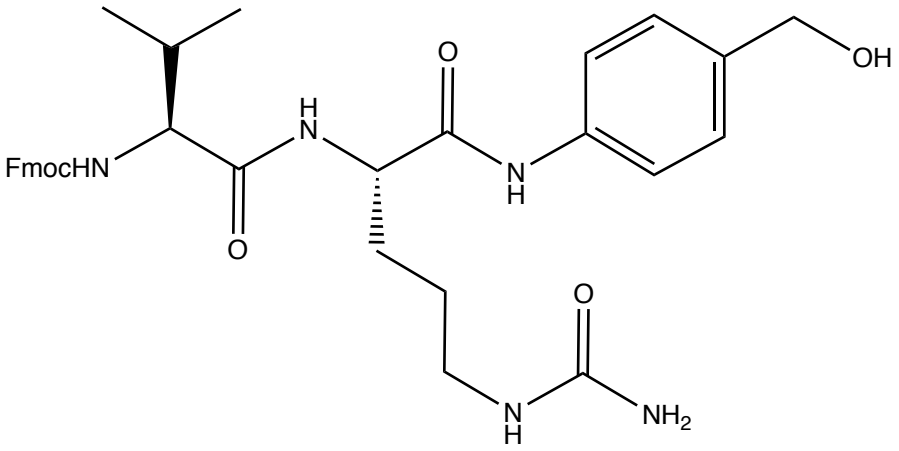

A solution of Fmoc-Cit-PABOH (0.594 g, 1.180 mmol, 1.00 eq) in DMF (0.2 M) was treated with trimethylamine (3.31 mL, 23.8 mmol, 20.1 eq). The reaction was stirred for 24 hours at room temperature. DMF and excess trimethylamine were removed under reduced pressure. Trace trimethylamine was removed by co-evaporation with DMF. The resulting residue was dissolved in DMF (0.1 M) and to the solution, Fmoc-Val-OSu (0.568 g, 1.30 mmol, 1.10 eq) was added. The reaction was stirred for 20 hours at room temperature. DMF was removed under reduced pressure and the resulting residue was purified by flash column chromatography using 3-12 % MeOH-DCM as solvent. Product was obtained as a white solid. (0.462 g, 0.767 mmol, 65 % yield). ^{1}H NMR (500 MHz, DMSO-d_6) δ 9.98 (s, 1H), 8.11 (d, J = 7.7 Hz, 1H), 7.89 (d, J = 7.6 Hz, 2H), 7.74 (dd, J = 10.2, 7.6 Hz, 2H), 7.54 (d, J = 8.2 Hz, 2H), 7.47 – 7.38 (m, 3H), 7.32 (dd, J = 7.5 Hz, 2H),

7.23 (d, J = 8.2 Hz, 2H), 5.97 (t, J = 5.9 Hz, 1H), 5.41 (s, 2H), 5.10 (t, J = 5.7 Hz, 1H), 4.45 – 4.39 (m, 3H), 4.34 – 4.19 (m, 3H), 3.93 (dd, J = 9.0, 7.0 Hz, 1H), 3.06 – 2.97 (m, 1H), 2.97 – 2.89 (m, 1H), 2.03 – 1.92 (m, 1H), 1.75 – 1.64 (m, 1H), 1.63 – 1.53 (m, 1H), 1.43 (q, J = 7.4, 5.6 Hz, 1H), 1.40 – 1.31 (m, 1H), 0.87 (dd, J = 14.0, 6.7 Hz, 6H).

Synthesis of Mc-Val-Cit-PABOH [18]

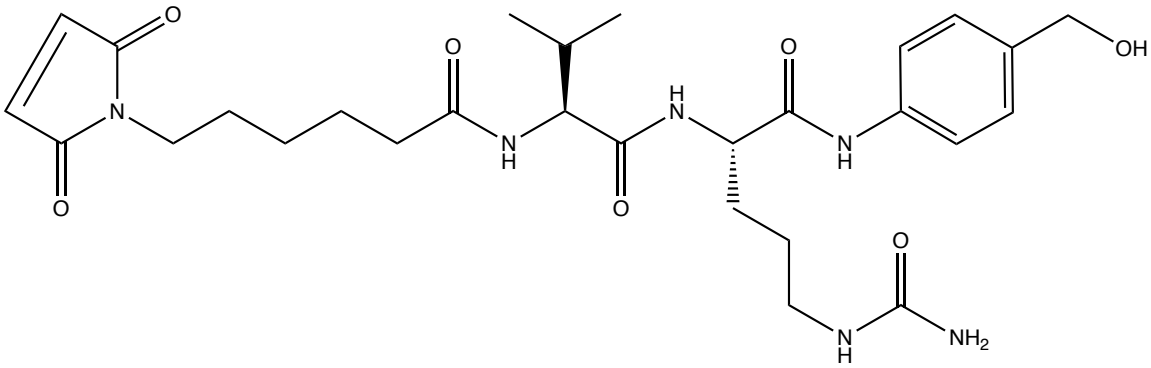

A solution of Fmoc-Val-Cit-PABOH (0.725g, 1.20 mmol, 1.00 eq) in DMF (0.2 M) was treated with trimethylamine (3.36 mL, 24.0 mmol, 20.0 eq). The reaction stirred for 24 hours at room temperature. DMF and excess trimethylamine was removed under reduced pressure. Trace trimethylamine was removed by co-evaporation with DMF. The resulting residue was dissolved in DMF (0.1 M) and to the solution, Mc-OSu (0.423 g, 1.37 mmol, 1.14 eq) was added. The reaction was stirred for 20 hours at room temperature. DMF was then removed under reduced pressure and the resulting residue was purified by flash column chromatography using 3-12% MeOH-DCM as solvent. Product was obtained as a white solid. (0.415g, 0.724 mmol, 60% yield). ^{1}H NMR (600 MHz, DMSO-d_6) δ 9.92 (s, 1H), 8.06 (d, J = 7.6 Hz, 1H), 7.82 (d, J = 8.7 Hz, 1H), 7.55 (d, 2H), 7.22 (d, 2H), 7.00 (s, 2H), 6.01 (t, J = 6.0 Hz, 1H), 5.42 (s, 2H), 5.09 (t, J = 5.7 Hz, 1H), 4.42 (d, J = 5.1 Hz,

2H), 4.40 – 4.30 (m, 1H), 4.18 (d, *J* = 8.6, 6.6 Hz, 1H), 3.05 – 2.97 (m, 1H), 2.97 – 2.89 (m, 1H), 2.22 – 2.05 (m, 2H), 2.00 – 1.89 (m, 1H), 1.75 – 1.63 (m, 1H), 1.63 – 1.53 (m, 1H), 1.53 – 1.39 (m, 5H), 1.39 – 1.30 (m, 1H), 1.21 – 1.09 (m, 3H), 0.83 (dd, 6H). HPLC: 90% pure.

Synthesis of Linker-Payload Construct

Synthesis of Mc-Val-Cit-PABC-KGP05 [18]

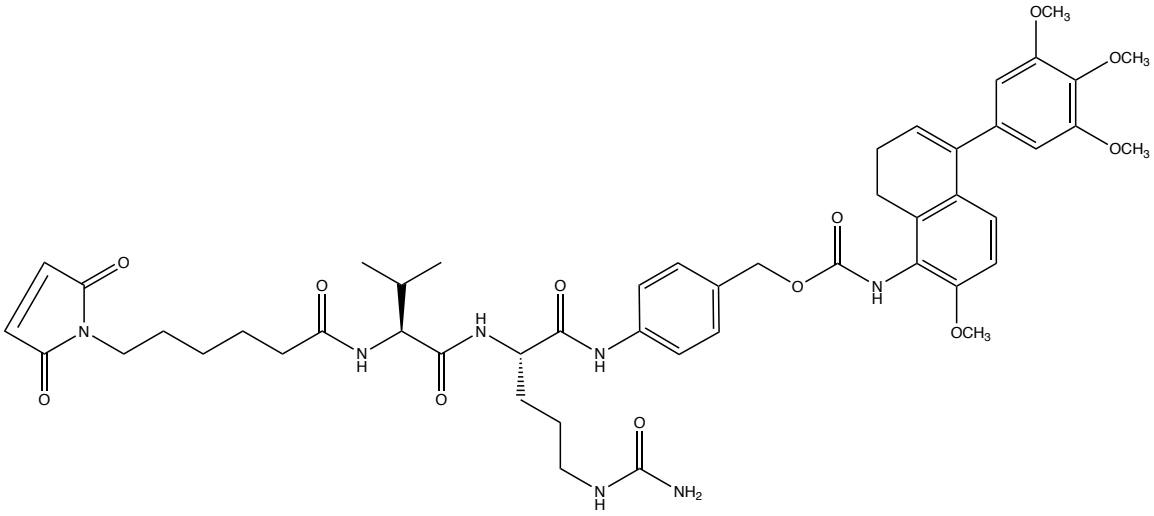

A solution of KGP05 (0.200 g, 0.586 mmol, 1.00 eq) in DCM (0.1 M)-$NaHCO_3$ Sat [1:1] was treated with triphosgene (0.521 g, 1.78 mmol, 3.00 eq). The reaction was stirred for 2 hours at room temperature to generate the desired isocyanate. The resulting residue was purified by flash column chromatography using 3-12% MeOH-DCM as solvent. The isocyanate was taken to the next step without further purification. A solution of Mc-Val-Cit-PABOH (0.205 g, 0.358 mmol, 1.00 eq) and the isocyanate compound (0.197 g, 0.537 mmol, 1.50 eq) in DMF (0.2 M) was treated with dibutyltin dilaurate (0.42 mL, 0.72 mmol, 2.0 eq). The reaction was stirred for 3 days at room temperature. DMF was removed under

reduced pressure and the resulting residue was purified by flash column chromatography using 3-12% MeOH-DCM as solvent. The product was obtained as a white solid. (0.028 g, 0.029 mmol, 5% yield). ^{1}H NMR (600 MHz, DMSO-d_6) δ 10.00 (s, 1H), 8.66 (s, 1H), 8.08 (d, J = 7.6 Hz, 1H), 7.80 (d, J = 8.6 Hz, 1H), 7.61 (s, 2H), 7.35 (s, 2H), 7.00 (s, 2H), 6.91 – 6.85 (m, 1H), 6.81 (d, J = 8.5 Hz, 1H), 6.55 (s, 2H), 5.97 (dd, J = 11.8, 5.8 Hz, 2H), 5.41 (s, 2H), 5.03 (d, J = 8.8 Hz, 2H), 4.38 (d, J = 6.9 Hz, 1H), 4.19 (dd, J = 8.6, 6.7 Hz, 1H), 3.75 (s, 5H), 3.73 (d, J = 6.2 Hz, 3H), 3.69 (s, 3H), 3.36 (t, J = 7.1 Hz, 2H), 3.02 (dd, J = 13.4, 6.7 Hz, 1H), 2.94 (p, J = 6.5 Hz, 1H), 2.62 (d, J = 8.0 Hz, 2H), 2.24 (s, 2H), 2.18 (td, J = 7.3, 2.7 Hz, 2H), 2.11 (dt, J = 17.0, 8.6 Hz, 1H), 1.96 (td, J = 13.5, 11.6, 4.9 Hz, 2H), 1.69 (s, 1H), 1.63 – 1.56 (m, 1H), 1.48 (q, J = 8.6 Hz, 6H), 1.35 (s, 2H), 1.18 (dd, J = 11.0, 4.5 Hz, 2H), 0.85 (dd, J = 6.8, 3.0 Hz, 3H), 0.82 (d, J = 6.8 Hz, 3H). ^{13}C NMR (151 MHz, DMSO) δ 172.72, 171.75, 171.53, 171.06, 159.33, 154.88, 153.15, 139.39, 137.13, 136.42, 134.91, 132.21, 127.89, 125.33, 124.78, 119.36, 108.83, 106.09, 60.50, 58.03, 56.32, 55.39, 53.57, 37.48, 35.41, 30.89, 29.77, 28.24, 26.26, 25.39, 24.97, 22.89, 22.57, 19.73, 18.67. HPLC: 84% pure.

CHAPTER THREE

Results and Discussion

Over the course of this study, the synthesis of Mc-Val-Cit-PABOH was performed with varying conditions to enhance the overall yield. Following the synthesis of the linker, the payload, KGP05, was attached with overall success.

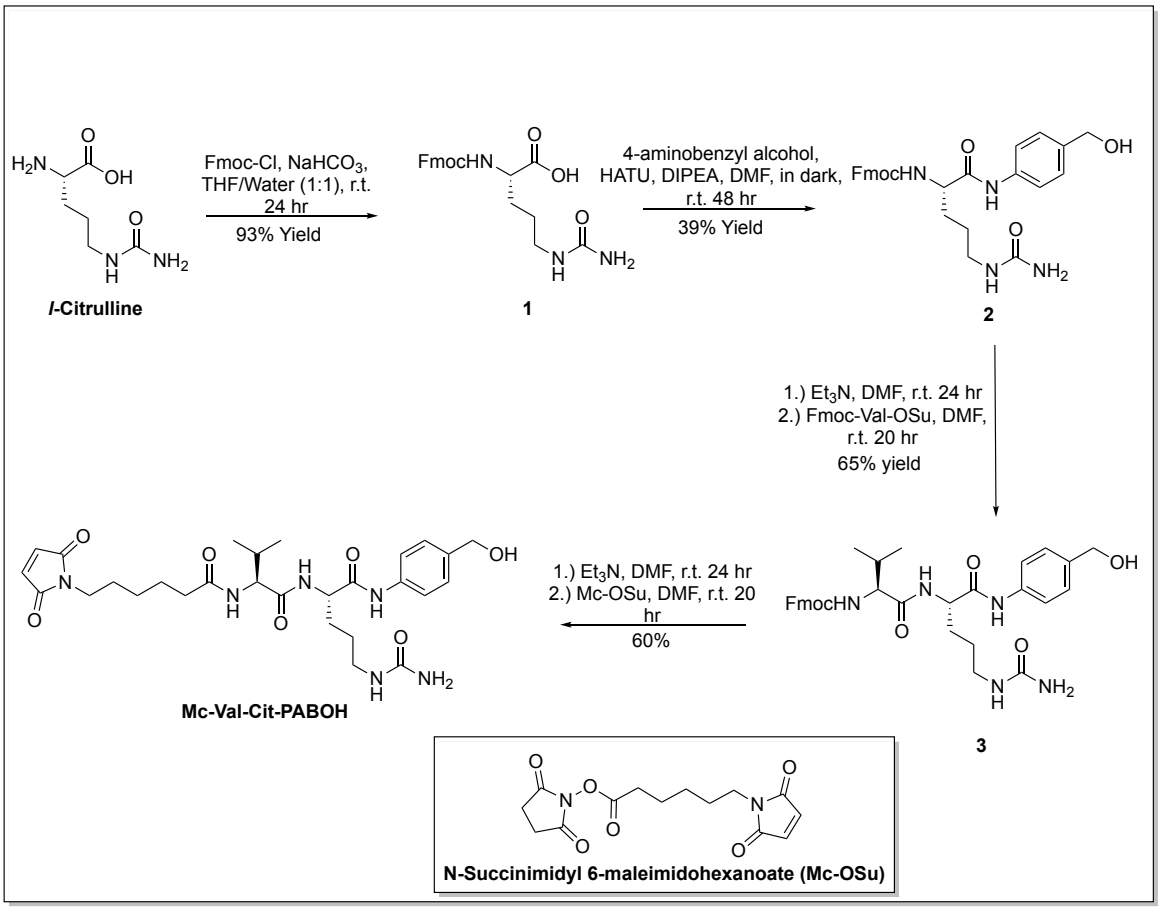

Scheme 1: Synthesis of Mc-Val-Cit-PABOH.

Figure 1 outlines the steps taken to prepare the peptide linker Mc-Val-Cit-PABOH. The first step resulted in successful addition of the protecting group Fmoc to the *l*-Citrulline amino acid resulting in compound **1** which was then subjected to a HATU coupling reaction to attach the *para*-amino benzyl alcohol to the C terminus of the amino acid. Next, Fmoc-Cit-PABOH, compound **2**, was treated with base to remove the Fmoc group. Now this position was open to accept the Fmoc protected valine amino acid in the next step of the reaction which resulted in compound **3**. This reaction had to be repeated as there was excess tri-ethyl amine (base) when reacting with Fmoc-Val which resulted in the undesired deprotection of the Valine amino acid. Compound **3** was then treated with base to deprotect and remove the Fmoc group from the Valine. Finally, the residue was reacted with Mc-OSu to yield the desired Mc-Val-Cit-PABOH compound. Each reaction in this synthesis was purified by flash column chromatography before moving to the next step. ^{1}H NMR analyses were conducted to properly characterize and confirm the reaction products. Also, an HPLC analysis was conducted on the final linker compound which was found to have 90% purity.

Following the synthesis of the dipeptide linker, the payload KGP05 was synthesized with the intent of attaching it to the linker in a later reaction. Scheme 2 outlines the synthesis of KGP05 which has been reported previously by the Pinney group.[13] To start off, compound **4**, 6-methoxy-1-tetralone, was nitrated to form two constitutional isomers, with one isomer being the desired product, compound **5**, called 5-nitro-6-methoxy-1-tetralone.[13] KGP05 was then obtained by reacting 5-bromo-1,2,3-trimethoxybenzene with *n*-butyllithium, followed by the addition of compound **5** dissolved in THF to form compound **6**.[13] The reaction of compound **6** with Zn in the presence of acetic acid resulted

in reduction of the nitro group, and following a subsequent condensation reaction, the desired product, KGP05, was obtained with a 72% yield.[13] Each reaction in this synthesis was purified by flash column chromatography before moving to the next step. ^{1}H NMR analyses were conducted to properly characterize and confirm the reaction products.

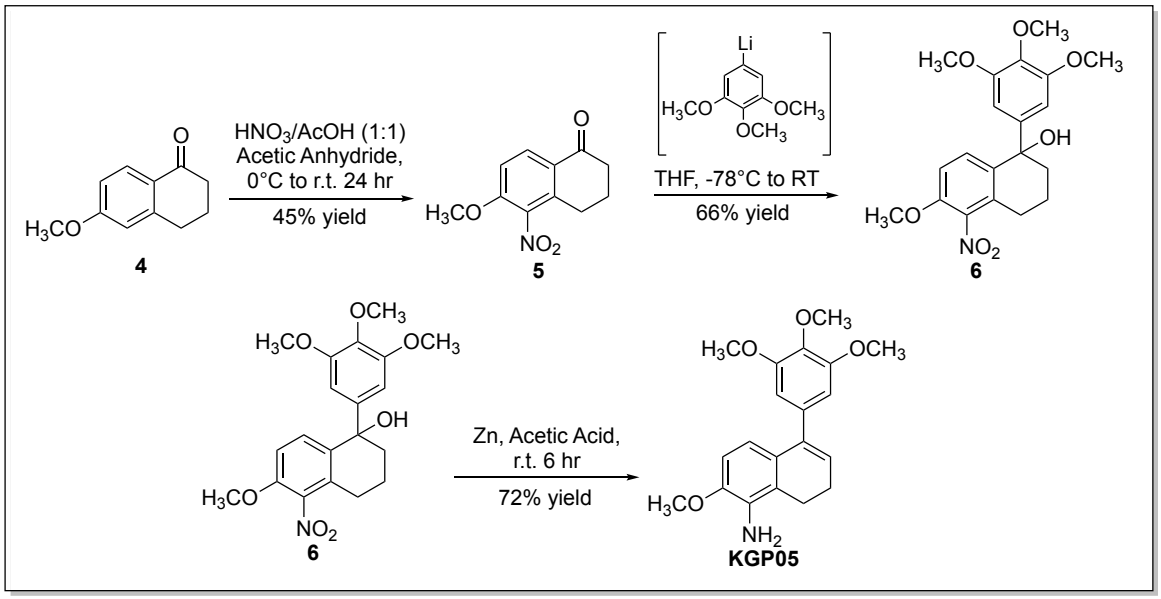

Scheme 2: Synthesis of KGP05.[13]

Upon successful synthesis of the linker (Mc-Val-Cit-PABOH) and payload (KGP05), the drug payload KGP05 was attached to yield a unique drug-linker construct ready to be evaluated for its specificity and cytotoxicity to human cancer cell lines by the Trawick Group. Scheme 3 displays the synthesis of Mc-Val-Cit-PABC-KGP05. Here, the KGP05 payload was reacted with triphosgene and sodium bicarbonate acting as the base in order to produce the isocyanate, compound **7**, through a carbonylation reaction.[48] Compound **7** was then mixed with the linker, Mc-Val-Cit-PABOH, with dibutyltin dilaurate, a catalyst. In this step, the isocyante of the payload reacts with the alcohol moiety

of the linker to produce the desired final drug-linker construct product, Mc-Val-Cit-PABC-KGP05. Each reaction in this synthesis was purified by flash column chromatography before moving to the next step. ^{1}H NMR analyses were conducted to properly characterize and confirm the reaction products. Also, ^{13}C NMR and HPLC analyses were conducted on the final drug-linker construct which was found to have 84% purity.

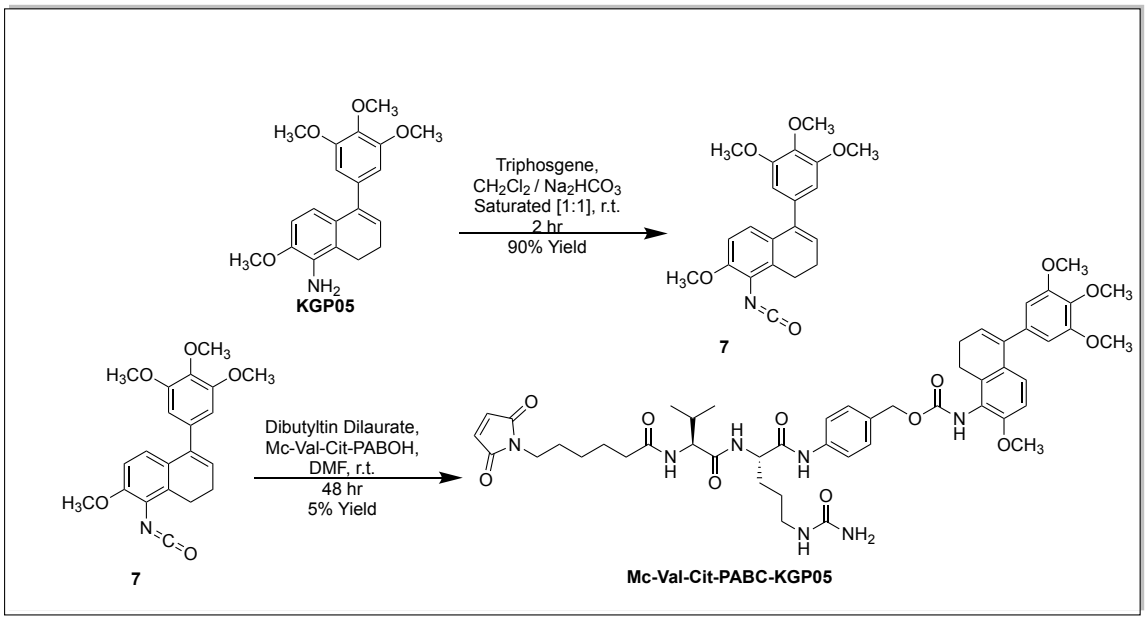

Scheme 3: Synthesis of KGP05 drug linker construct, Mc-Val-Cit-PABC-KGP05.

Next, the drug payload KGP18 was attempted to be attached to the linker through the process shown in Scheme 5. Upon analysis, it was determined that the desired product was not produced, but an undesired double addition of the KGP18-PNP on both sides of the linker occurred during the reaction. Upon analyzing this product by ESI mass spectrometry it was obvious that KGP18-PNP has reacted with not only the benzylic alcohol of the spacer but also with the free amine of the valine moiety of the dipeptide.

Scheme 4 and 5 display the synthetic process attempted to create KGP18 drug linker construct and the undesired product produced.

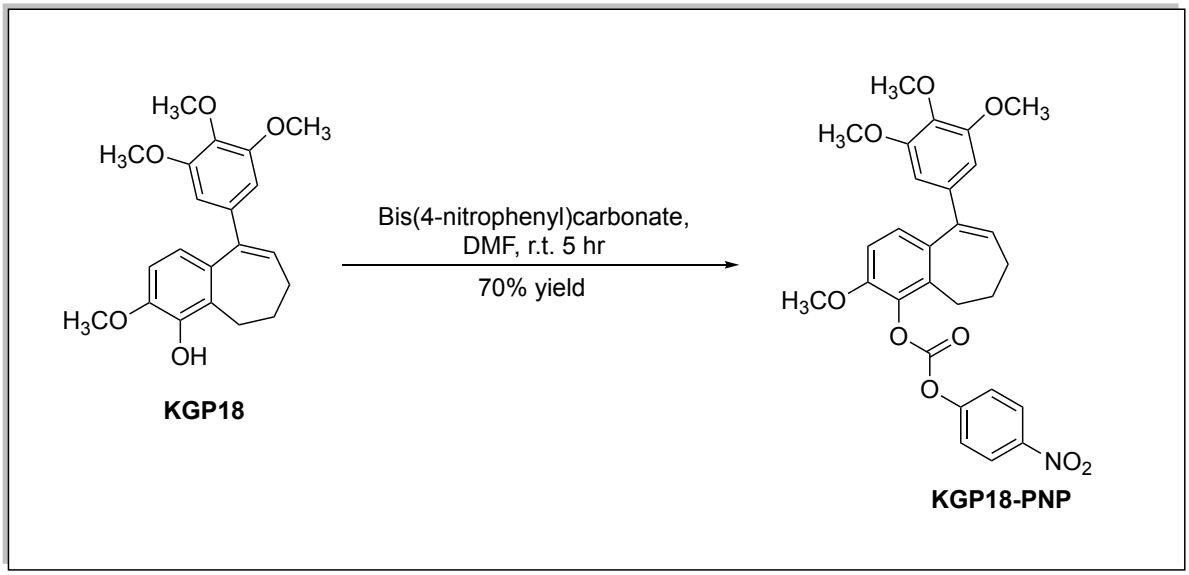

Scheme 4: Synthesis of KGP18-PNP.

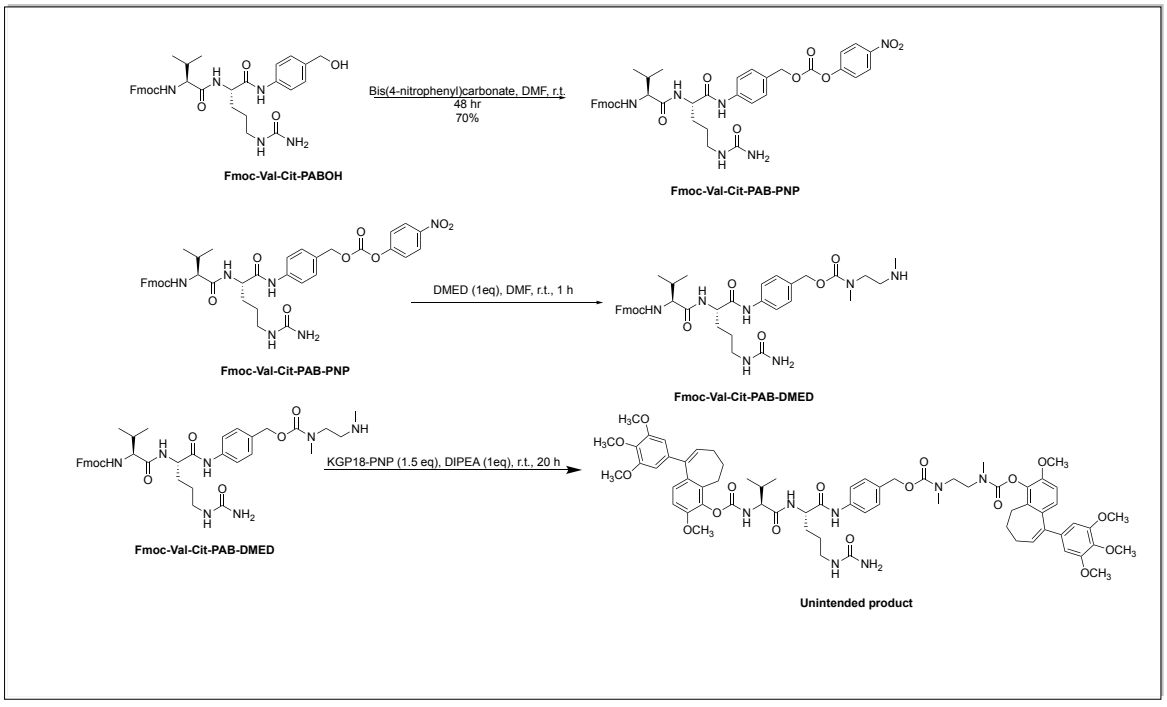

Scheme 5: Attempted synthesis of the KGP18 drug linker construct.

Scheme 6 outlines the next approach attempted in this synthesis to produce the desired KGP18 drug-linker construct. This proposed method used triethyl amine as the base rather than DIPEA in an effort to have more selectivity of KGP18-PNP addition onto the benzylic alcohol of the spacer rather than the free amine of the valine moiety of the dipeptide linker which becomes deprotected in the presence of base. While the desired KGP18 drug-linker construct was produced as confirmed by mass spectroscopy, an undesired side-product was also produced. Upon several purifications attempts by liquid column chromatography and prep TLC, the two compounds could not be separated from each other most likely due to their similarity in polarity.

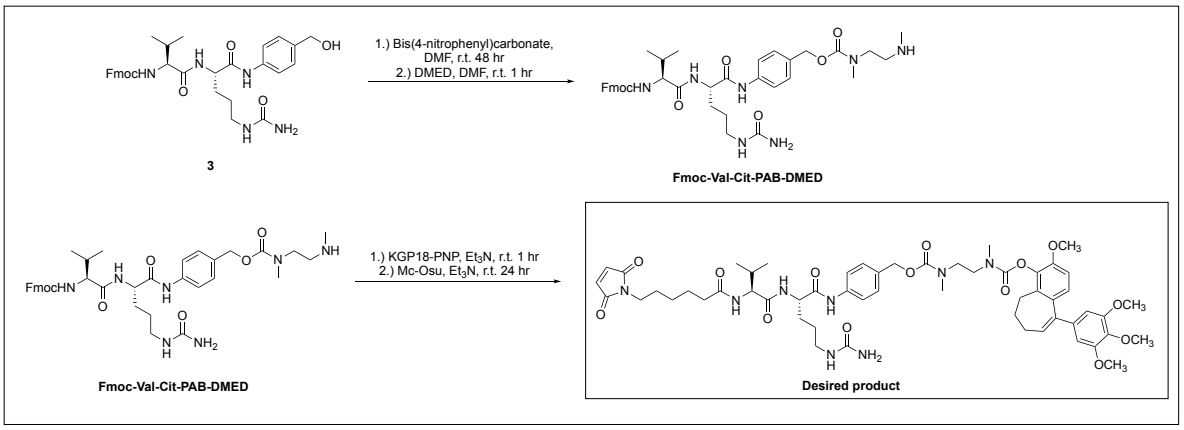

Scheme 6: Attempted synthesis of KGP18 drug-linker construct.

CHAPTER FOUR

Conclusions and Future Studies

The design and synthesis of new drug-linker constructs is vital for the successful preparation of a variety of ADCs. This study evaluates the synthesis of a peptide linker, VDA drug payloads, and their constructs. Future biological studies will be conducted on these drug-linker constructs to evaluate their cytotoxicity, inhibition of tubulin polymerization, and inhibition of the colchicine binding site. If these biological results show high cytotoxicity, cleavability, and specificity, then they could be paired to antibodies specific to antigens expressed in the tumor microenvironment to produce a unique ADC.

In future studies, an important way to increase the efficiency of these drug-linker constructs could be to add a moiety that increases the construct's water solubility. One strategy for increasing water solubility could be using amino acids in the linker like glycine and serine because these possess shorter hydrocarbon and polar side chains, are reported to be more readily water soluble and more likely to be cleaved due to their structural simplicity.[13, 49] Another strategy for increasing water solubility of the drug-linker construct could be by adding a hydrochloride salt moiety.[13, 50] There have been studies demonstrating that these salt payloads still have acute cytotoxicity and ability to inhibit tubulin polymerization.[24, 27] Further, an ADC synthesized to deliver glucocorticoids has shown success in using a phosphate bridge attached to the aliphatic alcohol of the linker to increase plasma stability while also maintaining rapid release of payload in the lysosomal environment.[52] This method could be applied to oncological drug-linker constructs in the future. While increasing water solubility would increase the stability of an ADC in the

blood, adding another step in the synthetic pathway of the drug-linker construct could lead to a decrease in overall yield or the synthesis of a bulky molecule with low stability. These are problems future scientists in the Pinney lab and beyond will have to tackle in the coming years.

The goal to synthesize pure KGP18 drug-linker construct was unsuccessful in this study, but has been successfully achieved by the Pinney Group in the past. In the attempted synthetic approach, the desired product along with an undesired side product were obtained and these two molecules were unable to be separated from each other during the course of these studies. In the future, the hope is to apply the knowledge gained from this study in order to devise and test an alternate synthetic route which minimizes or inhibits the double addition of the KGP18 prodrug to the linker or the production of the inseparable side-product. These studies focused on the synthesis of the VDA payloads, KGP05 and KGP18; the linker, Mc-Val-Cit-PABOH; and their unique drug-linker constructs as a cleavable tubulin inhibitor anti-cancer therapeutic. While there were obstacles faced along the way, these reported methods proved to be efficient and provided good yields for the final drug-linker construct.

APPENDIX

Appendix A: NMR Spectra

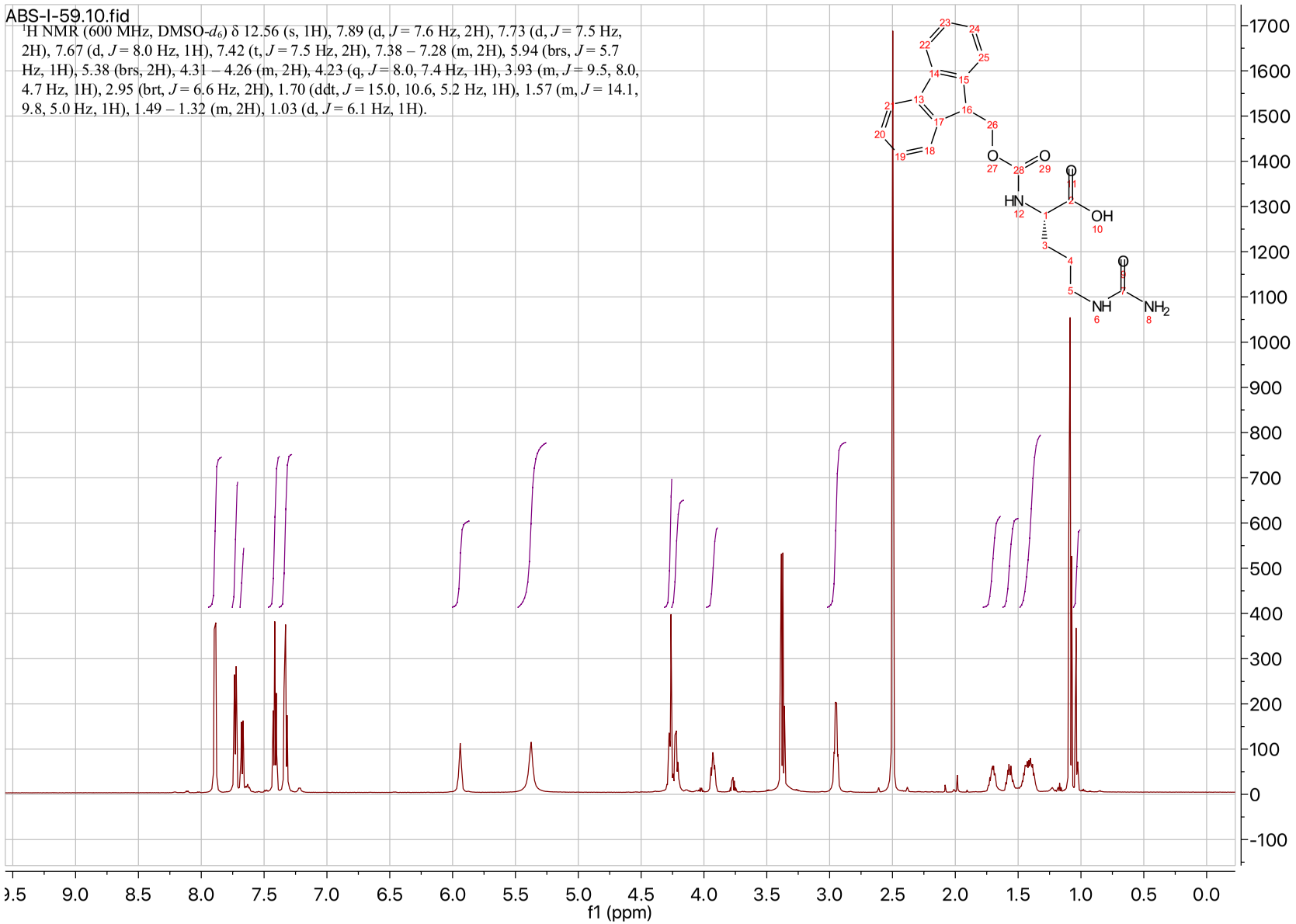
ABS-I-59.10.fid
^{1}H NMR (600 MHz, DMSO-d_6) δ 12.56 (s, 1H), 7.89 (d, J = 7.6 Hz, 2H), 7.73 (d, J = 7.5 Hz, 2H), 7.67 (d, J = 8.0 Hz, 1H), 7.42 (t, J = 7.5 Hz, 2H), 7.38 – 7.28 (m, 2H), 5.94 (brs, J = 5.7 Hz, 1H), 5.38 (brs, 2H), 4.31 – 4.26 (m, 2H), 4.23 (q, J = 8.0, 7.4 Hz, 1H), 3.93 (m, J = 9.5, 8.0, 4.7 Hz, 1H), 2.95 (brt, J = 6.6 Hz, 2H), 1.70 (ddt, J = 15.0, 10.6, 5.2 Hz, 1H), 1.57 (m, J = 14.1, 9.8, 5.0 Hz, 1H), 1.49 – 1.32 (m, 2H), 1.03 (d, J = 6.1 Hz, 1H).
f1 (ppm)

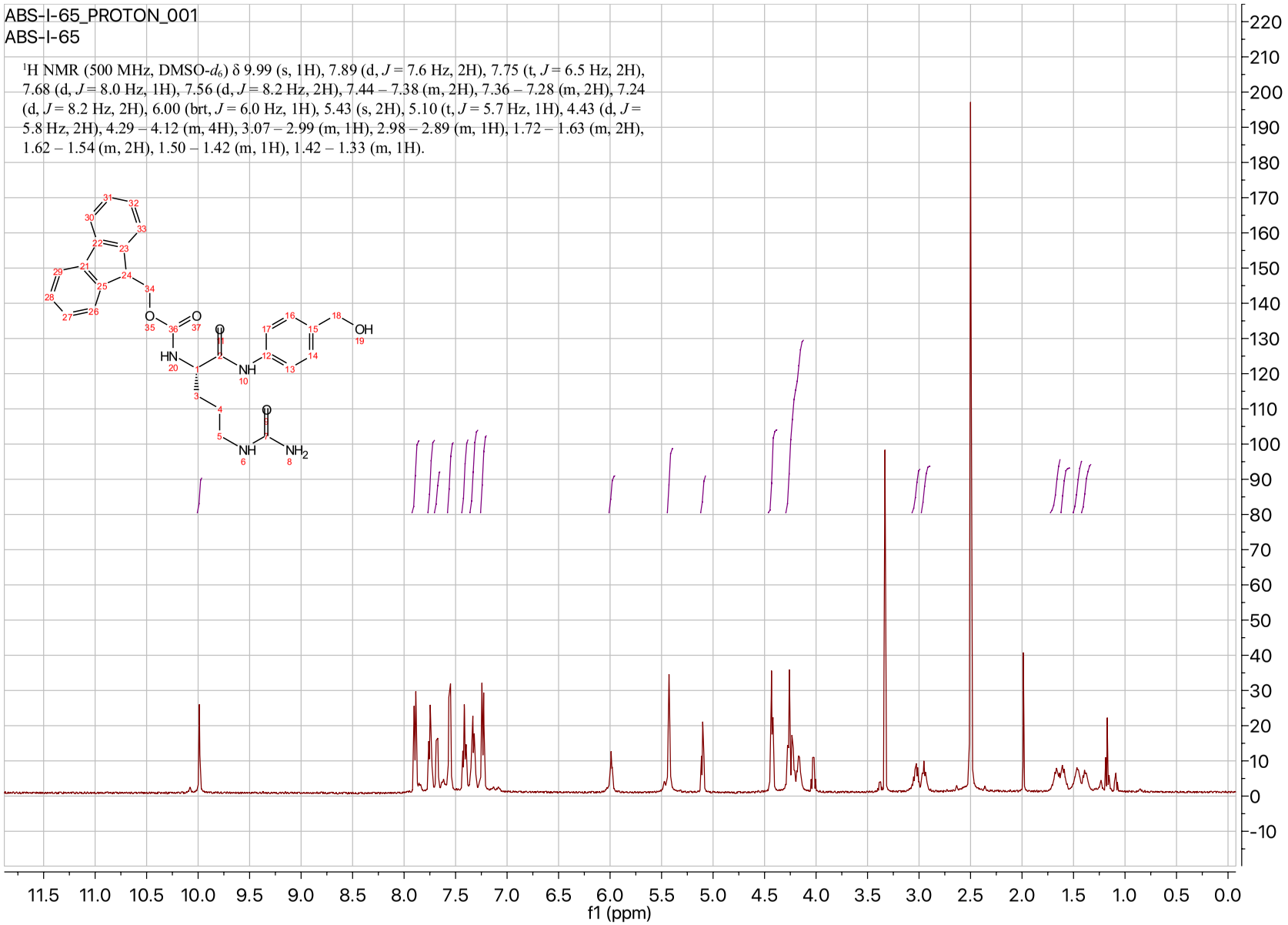
ABS-I-65_PROTON_001
ABS-I-65
[1]H NMR (500 MHz, DMSO-d_6) δ 9.99 (s, 1H), 7.89 (d, J = 7.6 Hz, 2H), 7.75 (t, J = 6.5 Hz, 2H), 7.68 (d, J = 8.0 Hz, 1H), 7.56 (d, J = 8.2 Hz, 2H), 7.44 – 7.38 (m, 2H), 7.36 – 7.28 (m, 2H), 7.24 (d, J = 8.2 Hz, 2H), 6.00 (brt, J = 6.0 Hz, 1H), 5.43 (s, 2H), 5.10 (t, J = 5.7 Hz, 1H), 4.43 (d, J = 5.8 Hz, 2H), 4.29 – 4.12 (m, 4H), 3.07 – 2.99 (m, 1H), 2.98 – 2.89 (m, 1H), 1.72 – 1.63 (m, 2H), 1.62 – 1.54 (m, 2H), 1.50 – 1.42 (m, 1H), 1.42 – 1.33 (m, 1H).
OH
HN
NH
NH
NH2
O
f1 (ppm)

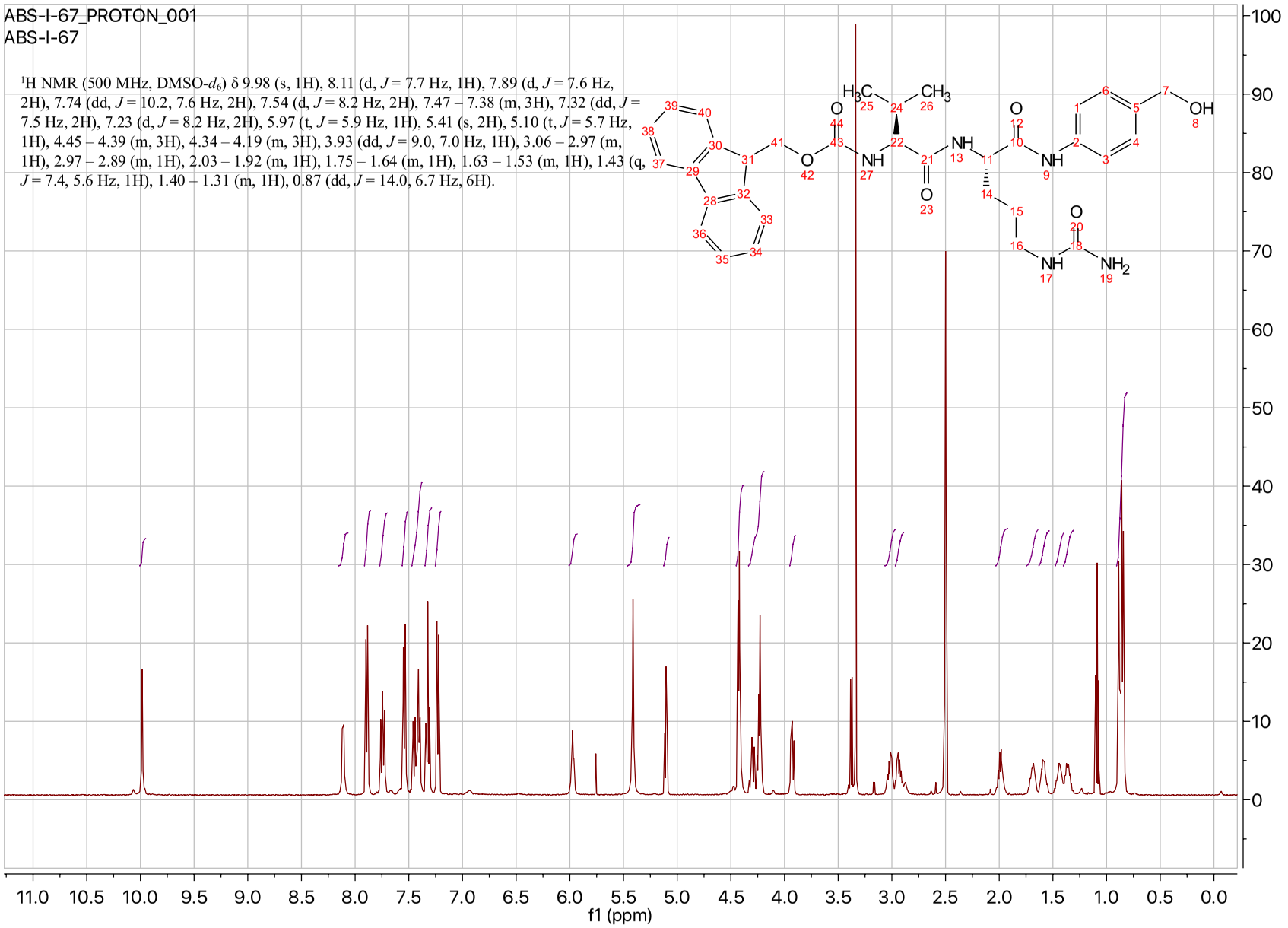
ABS-I-67_PROTON_001
ABS-I-67
[1]H NMR (500 MHz, DMSO-d_6) δ 9.98 (s, 1H), 8.11 (d, J = 7.7 Hz, 1H), 7.89 (d, J = 7.6 Hz, 2H), 7.74 (dd, J = 10.2, 7.6 Hz, 2H), 7.54 (d, J = 8.2 Hz, 2H), 7.47 – 7.38 (m, 3H), 7.32 (dd, J = 7.5 Hz, 2H), 7.23 (d, J = 8.2 Hz, 2H), 5.97 (t, J = 5.9 Hz, 1H), 5.41 (s, 2H), 5.10 (t, J = 5.7 Hz, 1H), 4.45 – 4.39 (m, 3H), 4.34 – 4.19 (m, 3H), 3.93 (dd, J = 9.0, 7.0 Hz, 1H), 3.06 – 2.97 (m, 1H), 2.97 – 2.89 (m, 1H), 2.03 – 1.92 (m, 1H), 1.75 – 1.64 (m, 1H), 1.63 – 1.53 (m, 1H), 1.43 (q, J = 7.4, 5.6 Hz, 1H), 1.40 – 1.31 (m, 1H), 0.87 (dd, J = 14.0, 6.7 Hz, 6H).
f1 (ppm)

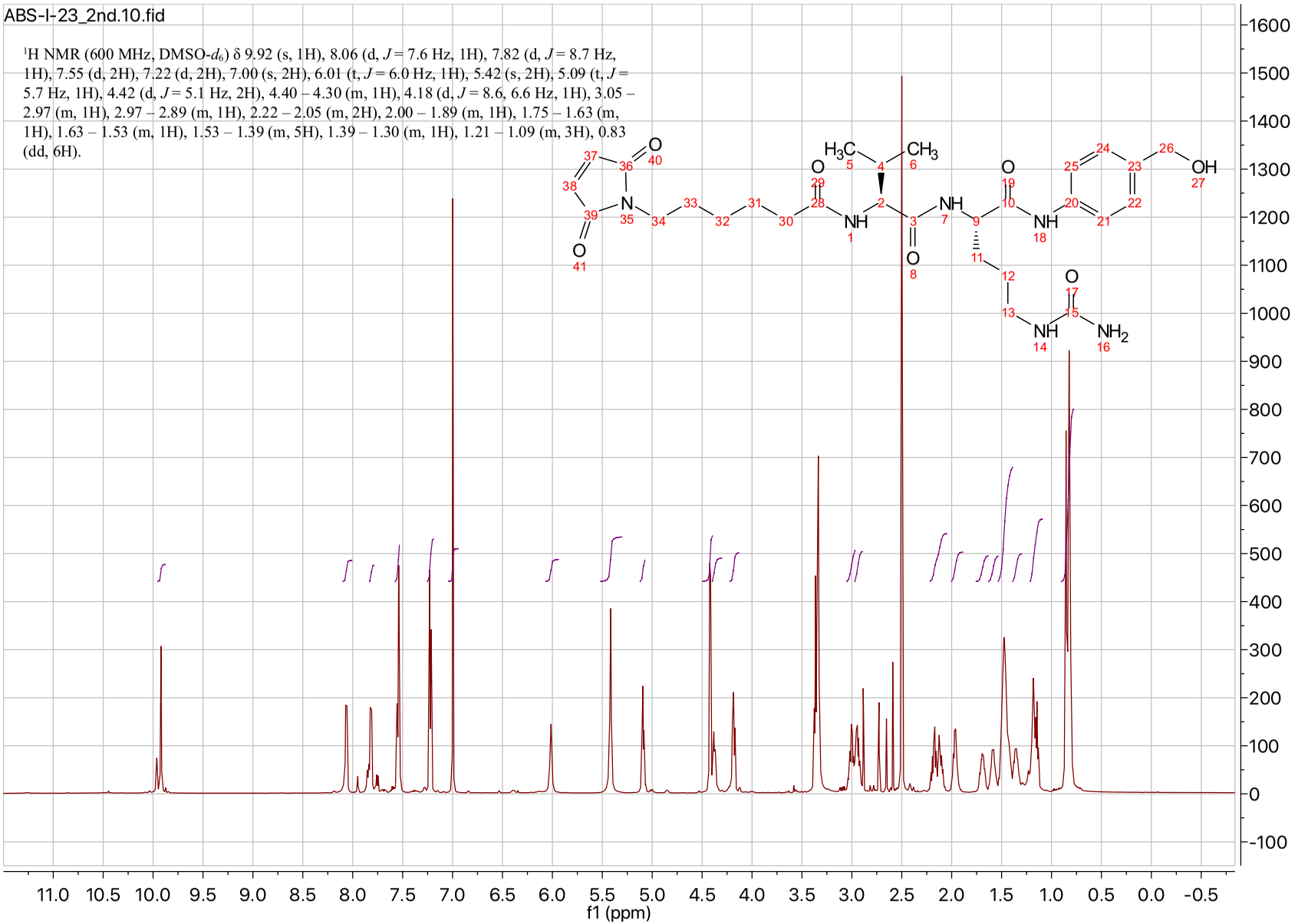
ABS-I-23_2nd.10.fid
^{1}H NMR (600 MHz, DMSO-d_6) δ 9.92 (s, 1H), 8.06 (d, J = 7.6 Hz, 1H), 7.82 (d, J = 8.7 Hz, 1H), 7.55 (d, 2H), 7.22 (d, 2H), 7.00 (s, 2H), 6.01 (t, J = 6.0 Hz, 1H), 5.42 (s, 2H), 5.09 (t, J = 5.7 Hz, 1H), 4.42 (d, J = 5.1 Hz, 2H), 4.40 – 4.30 (m, 1H), 4.18 (d, J = 8.6, 6.6 Hz, 1H), 3.05 – 2.97 (m, 1H), 2.97 – 2.89 (m, 1H), 2.22 – 2.05 (m, 2H), 2.00 – 1.89 (m, 1H), 1.75 – 1.63 (m, 1H), 1.63 – 1.53 (m, 1H), 1.53 – 1.39 (m, 5H), 1.39 – 1.30 (m, 1H), 1.21 – 1.09 (m, 3H), 0.83 (dd, 6H).
f1 (ppm)

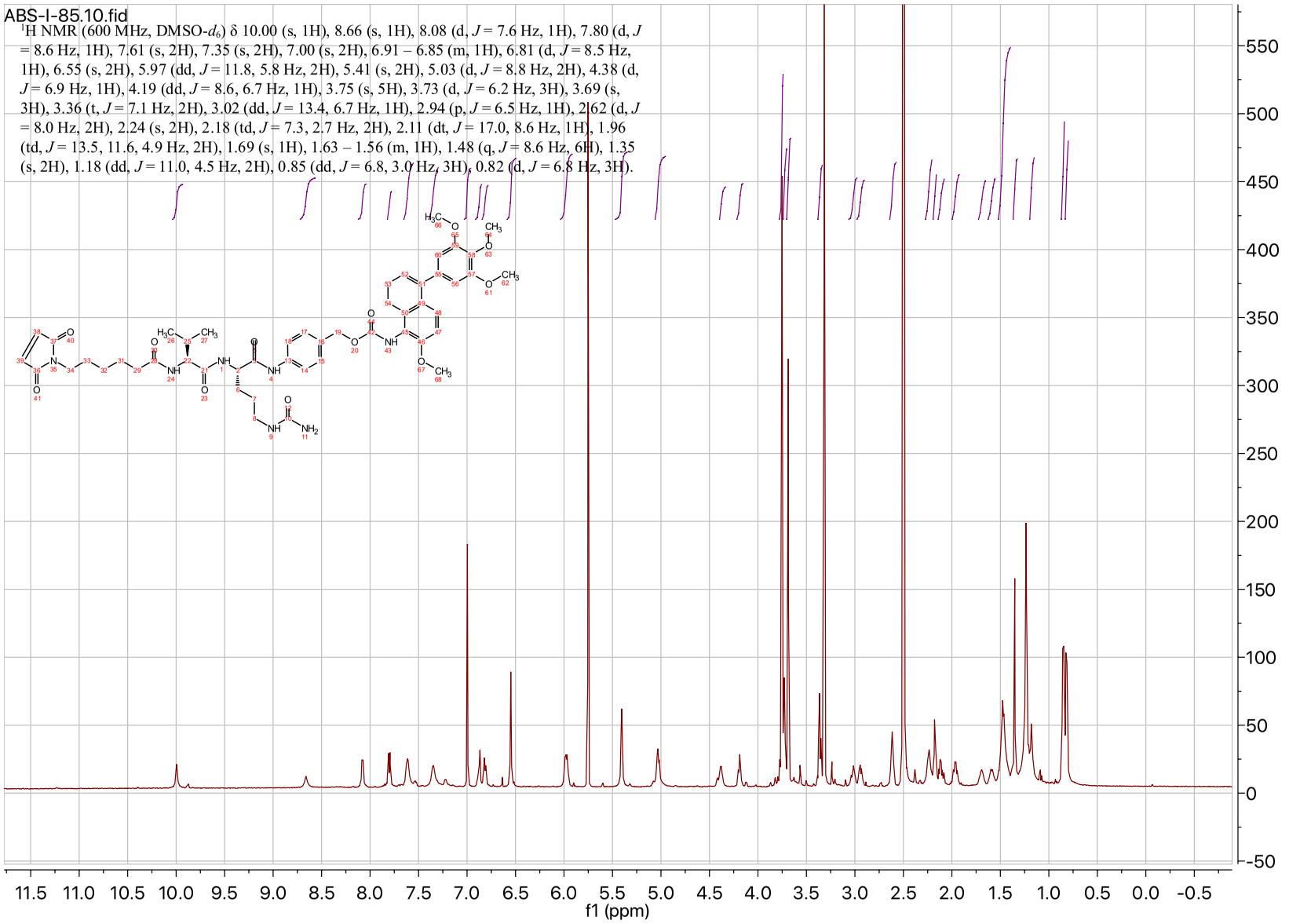
ABS-I-85.10.fid
^{1}H NMR (600 MHz, DMSO-d_6) δ 10.00 (s, 1H), 8.66 (s, 1H), 8.08 (d, J = 7.6 Hz, 1H), 7.80 (d, J = 8.6 Hz, 1H), 7.61 (s, 2H), 7.35 (s, 2H), 7.00 (s, 2H), 6.91 – 6.85 (m, 1H), 6.81 (d, J = 8.5 Hz, 1H), 6.55 (s, 2H), 5.97 (dd, J = 11.8, 5.8 Hz, 2H), 5.41 (s, 2H), 5.03 (d, J = 8.8 Hz, 2H), 4.38 (d, J = 6.9 Hz, 1H), 4.19 (dd, J = 8.6, 6.7 Hz, 1H), 3.75 (s, 5H), 3.73 (d, J = 6.2 Hz, 3H), 3.69 (s, 3H), 3.36 (t, J = 7.1 Hz, 2H), 3.02 (dd, J = 13.4, 6.7 Hz, 1H), 2.94 (p, J = 6.5 Hz, 1H), 2.62 (d, J = 8.0 Hz, 2H), 2.24 (s, 2H), 2.18 (td, J = 7.3, 2.7 Hz, 2H), 2.11 (dt, J = 17.0, 8.6 Hz, 1H), 1.96 (td, J = 13.5, 11.6, 4.9 Hz, 2H), 1.69 (s, 1H), 1.63 – 1.56 (m, 1H), 1.48 (q, J = 8.6 Hz, 6H), 1.35 (s, 2H), 1.18 (dd, J = 11.0, 4.5 Hz, 2H), 0.85 (dd, J = 6.8, 3.0 Hz, 3H), 0.82 (d, J = 6.8 Hz, 3H).
550
500
450
400
350
300
250
200
150
100
50
0
-50
11.5 11.0 10.5 10.0 9.5 9.0 8.5 8.0 7.5 7.0 6.5 6.0 5.5 5.0 4.5 4.0 3.5 3.0 2.5 2.0 1.5 1.0 0.5 0.0 -0.5
f1 (ppm)

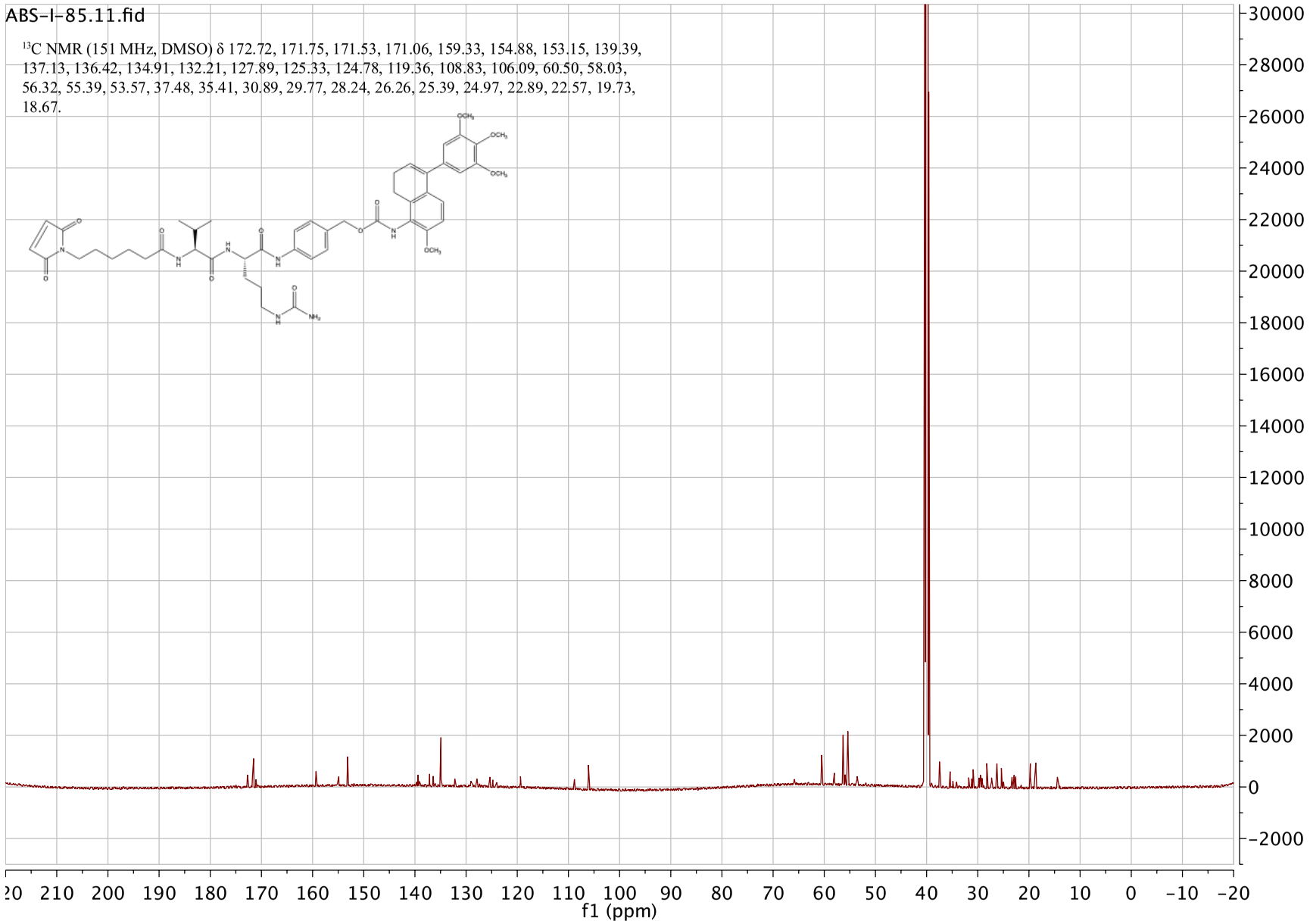
ABS-I-85.11.fid
13C NMR (151 MHz, DMSO) δ 172.72, 171.75, 171.53, 171.06, 159.33, 154.88, 153.15, 139.39, 137.13, 136.42, 134.91, 132.21, 127.89, 125.33, 124.78, 119.36, 108.83, 106.09, 60.50, 58.03, 56.32, 55.39, 53.57, 37.48, 35.41, 30.89, 29.77, 28.24, 26.26, 25.39, 24.97, 22.89, 22.57, 19.73, 18.67.
30000
28000
26000
24000
22000
20000
18000
16000
14000
12000
10000
8000
6000
4000
2000
0
-2000
210 200 190 180 170 160 150 140 130 120 110 100 90 80 70 60 50 40 30 20 10 0 -10 -20
f1 (ppm)

Appendix B: HPLC Data

Mc-Val-Cit-PABOH: 90% Pure

Data File C:\Chem32\1\Data\Jake\ABS-I-75.D
Sample Name: ABS-I-75

Acq. Operator : SYSTEM
Sample Operator : SYSTEM
Acq. Instrument : 1200 HPLC Location : 1
Injection Date : 7/13/2019 4:57:13 PM
Inj Volume : No inj
Acq. Method : C:\Chem32\1\Methods\GRAD 2 50-90 ACN.M
Last changed : 4/30/2014 1:53:57 AM by ERICAP
Analysis Method : C:\Chem32\1\Methods\MASTERMETHOD2.M
Last changed : 12/2/2015 12:37:42 PM by Eric Lin
Sample Info : MC-Val-Cit-PABOH (ABS-I-75)

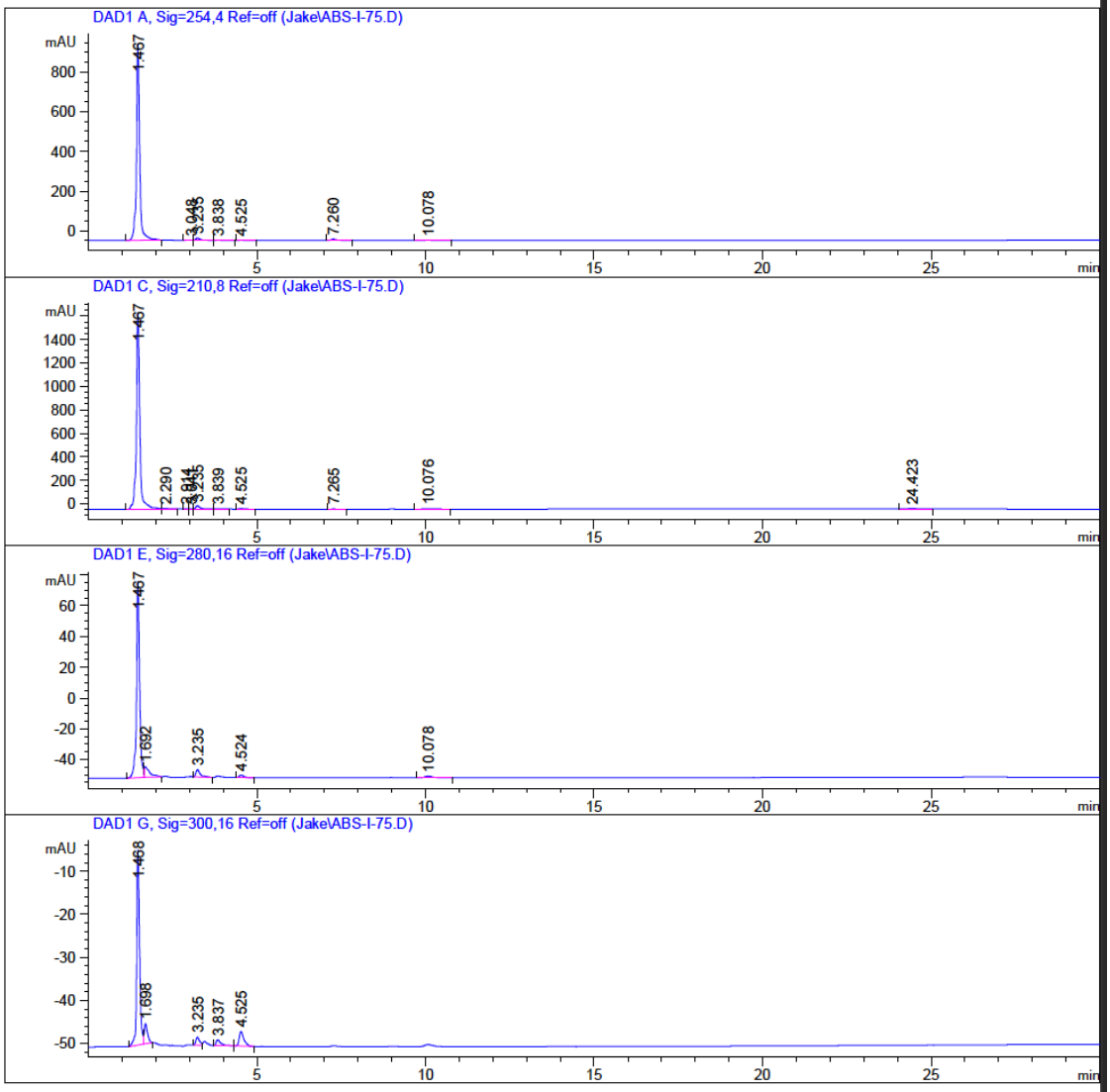

1200 HPLC 7/15/2019 10:28:48 AM SYSTEM Page 1 of 3

Data File C:\Chem32\1\Data\Jake\ABS-I-75.D
Sample Name: ABS-I-75

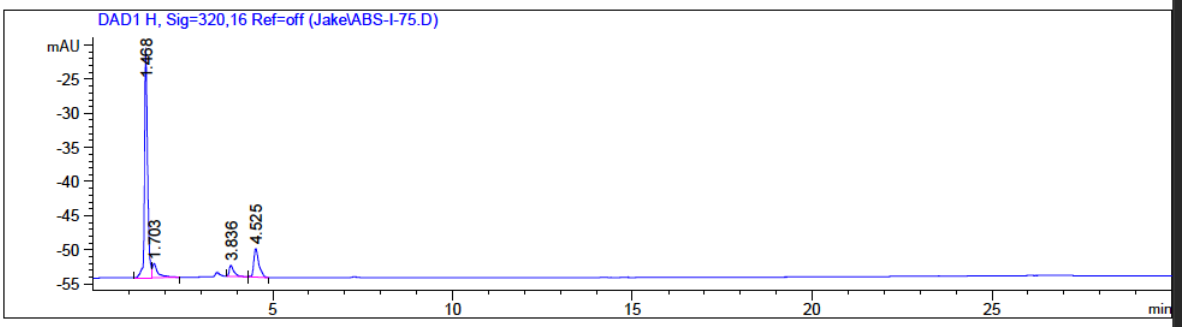

==========

Area Percent Report

==========

Sorted By : Signal
Multiplier : 1.0000
Dilution : 1.0000
Sample Amount: : 1.00000 [ng/ul] (not used in calc.)
Use Multiplier & Dilution Factor with ISTDs

Signal 1: DAD1 A, Sig=254,4 Ref=off

Peak #	RetTime [min]	Type	Width [min]	Area [mAU*s]	Height [mAU]	Area %
1	1.467	BB	0.0916	6455.05371	996.19574	96.1627
2	3.048	BV	0.1429	13.72619	1.32496	0.2045
3	3.235	VV	0.1412	110.01940	11.33673	1.6390
4	3.838	VB	0.1633	12.89438	1.11212	0.1921
5	4.525	BB	0.1454	13.41488	1.33347	0.1998
6	7.260	BB	0.1903	79.12875	6.06225	1.1788
7	10.078	BB	0.2678	28.40033	1.53519	0.4231
Totals :				6712.63764	1018.90046	

Signal 2: DAD1 C, Sig=210,8 Ref=off

Peak #	RetTime [min]	Type	Width [min]	Area [mAU*s]	Height [mAU]	Area %
1	1.467	BV	0.1030	1.16916e4	1683.49255	95.1412
2	2.290	VB	0.1827	65.13793	4.91289	0.5301
3	2.914	BV	0.0968	20.14769	3.22897	0.1640
4	3.041	VV	0.0976	20.67145	3.10874	0.1682
5	3.235	VB	0.1393	264.61975	27.73666	2.1534
6	3.839	BB	0.1446	34.34644	3.43550	0.2795
7	4.525	BB	0.1416	55.25455	5.67673	0.4496
8	7.265	BB	0.1998	15.66669	1.14405	0.1275
9	10.076	BB	0.2804	78.81969	4.09758	0.6414
10	24.423	BB	0.3049	42.41915	2.02081	0.3452

Data File C:\Chem32\1\Data\Jake\ABS-I-75.D
Sample Name: ABS-I-75

Totals : 1.22886e4 1738.85447

Signal 3: DAD1 E, Sig=280,16 Ref=off

Peak #	RetTime [min]	Type	Width [min]	Area [mAU*s]	Height [mAU]	Area %
1	1.467	BV	0.0885	796.15808	128.10965	83.0364
2	1.692	VB	0.1511	81.38235	7.02850	8.4879
3	3.235	BB	0.1358	44.12374	4.77422	4.6019
4	4.524	BB	0.1394	16.31908	1.70852	1.7020
5	10.078	BB	0.2622	20.82310	1.15565	2.1718

Totals : 958.80636 142.77654

Signal 4: DAD1 G, Sig=300,16 Ref=off

Peak #	RetTime [min]	Type	Width [min]	Area [mAU*s]	Height [mAU]	Area %
1	1.468	BV	0.0834	262.36572	45.40654	73.9776
2	1.698	VB	0.0980	31.98127	4.66147	9.0176
3	3.235	BV	0.1197	14.69276	1.86862	4.1428
4	3.837	BB	0.1365	12.86430	1.38264	3.6273
5	4.525	BB	0.1422	32.75137	3.40603	9.2347

Totals : 354.65543 56.72530

Signal 5: DAD1 H, Sig=320,16 Ref=off

Peak #	RetTime [min]	Type	Width [min]	Area [mAU*s]	Height [mAU]	Area %
1	1.468	BV	0.0832	192.66597	33.43027	72.1637
2	1.703	VB	0.1373	20.76944	2.06575	7.7793
3	3.836	BB	0.1280	13.97581	1.59794	5.2347
4	4.525	BB	0.1414	39.57329	4.14356	14.8223

Totals : 266.98451 41.23752

==========

*** End of Report ***

Mc-Val-Cit-PABC-KGP05: 84% Pure

Data File C:\Chem32\1\Data\Jake\ABS-I-99.D
Sample Name: ABS-I-99

Acq. Operator : SYSTEM
Sample Operator : SYSTEM
Acq. Instrument : 1200 HPLC Location : 1
Injection Date : 6/19/2019 12:36:32 PM
Inj Volume : No inj
Acq. Method : C:\Chem32\1\Methods\GRAD 2 50-90 ACN.M
Last changed : 4/30/2014 1:53:57 AM by ERICAP
Analysis Method : C:\Chem32\1\Methods\MASTERMETHOD2.M
Last changed : 12/2/2015 12:37:42 PM by Eric Lin

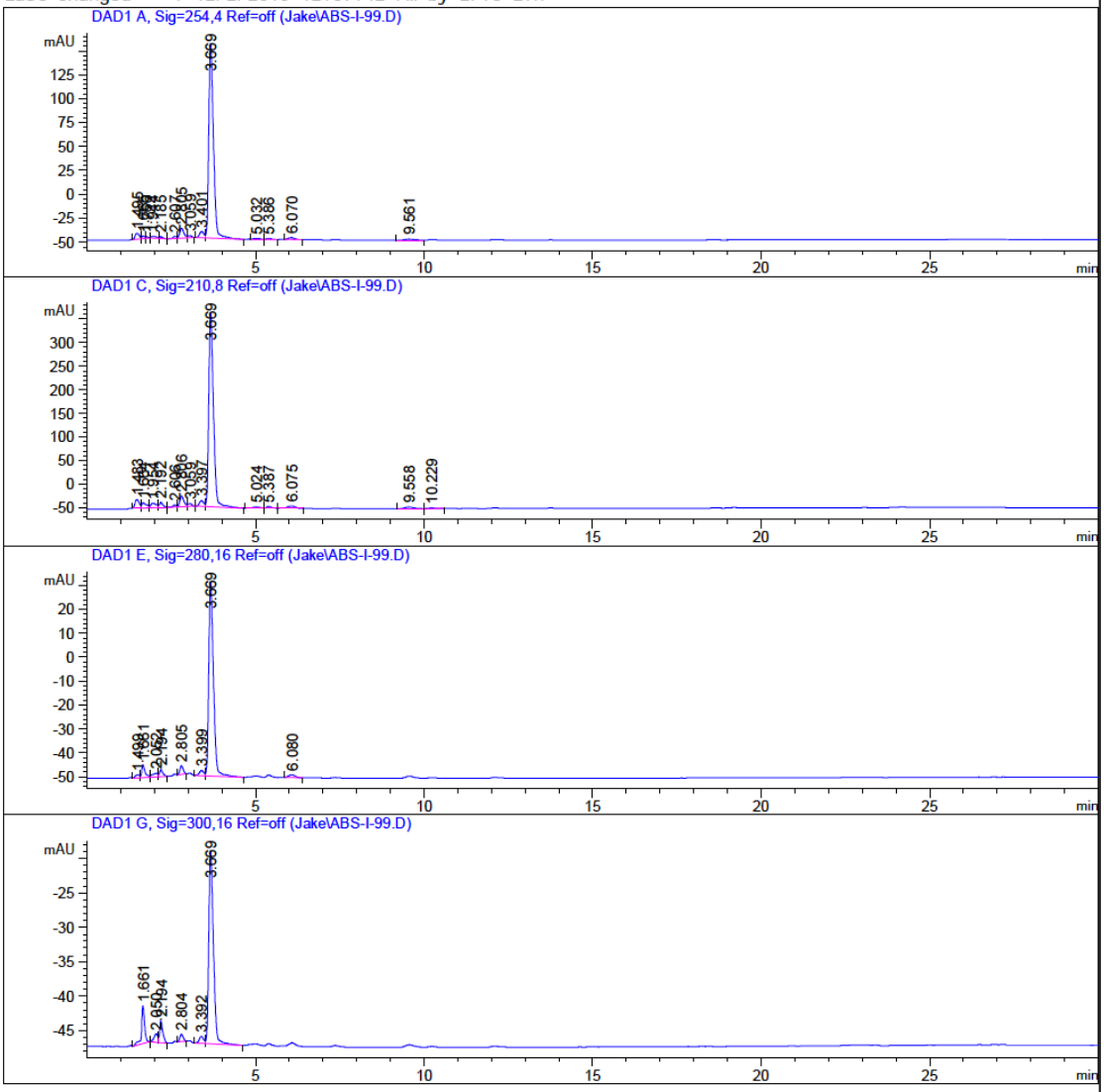

1200 HPLC 7/15/2019 10:08:20 AM SYSTEM Page 1 of 4

Data File C:\Chem32\1\Data\Jake\ABS-I-99.D
Sample Name: ABS-I-99

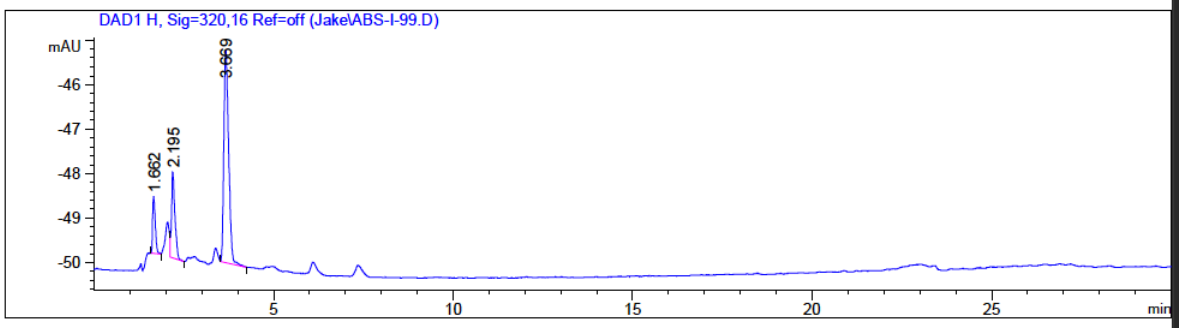

==========

Area Percent Report

==========

Sorted By : Signal
Multiplier : 1.0000
Dilution : 1.0000
Sample Amount: : 1.00000 [ng/ul] (not used in calc.)
Use Multiplier & Dilution Factor with ISTDs

Signal 1: DAD1 A, Sig=254,4 Ref=off

Peak #	RetTime [min]	Type	Width [min]	Area [mAU*s]	Height [mAU]	Area %
1	1.495	BV	0.1131	54.22970	6.38362	2.3489
2	1.665	VV	0.0888	17.06932	2.73506	0.7393
3	1.766	VB	0.0647	7.00096	1.61192	0.3032
4	1.944	BV	0.1724	21.39836	1.77838	0.9269
5	2.185	VB	0.1032	13.52821	1.89746	0.5860
6	2.607	BV	0.1135	16.43190	2.14274	0.7117
7	2.805	VV	0.1244	88.95795	10.54220	3.8532
8	3.059	VB	0.1265	19.16593	2.22500	0.8302
9	3.401	BV	0.1343	60.09003	6.72206	2.6028
10	3.669	VB	0.1409	1937.25708	203.76689	83.9110
11	5.032	BV	0.1805	11.81313	1.05618	0.5117
12	5.386	VB	0.1417	12.22289	1.32429	0.5294
13	6.070	BB	0.2242	28.76205	2.06884	1.2458
14	9.561	BB	0.2618	20.77636	1.18959	0.8999
Totals :				2308.70389	245.44426	

Signal 2: DAD1 C, Sig=210,8 Ref=off

Peak #	RetTime [min]	Type	Width [min]	Area [mAU*s]	Height [mAU]	Area %
1	1.483	BV	0.1296	161.31943	18.90460	3.2182
2	1.664	VV	0.1334	115.15079	11.64610	2.2972
3	1.954	VV	0.1738	115.66602	9.38527	2.3075
4	2.192	VB	0.1016	79.51984	11.09081	1.5864

Data File C:\Chem32\1\Data\Jake\ABS-I-99.D
Sample Name: ABS-I-99

Peak #	RetTime [min]	Type	Width [min]	Area [mAU*s]	Height [mAU]	Area %
5	2.606	BV	0.1133	31.54139	4.12077	0.6292
6	2.806	VV	0.1222	190.00183	23.03302	3.7904
7	3.059	VB	0.1316	49.92138	5.62284	0.9959
8	3.397	BV	0.1362	110.18508	12.33825	2.1981
9	3.669	VB	0.1406	3911.42358	412.57855	78.0300
10	5.024	BV	0.2483	42.98986	2.52891	0.8576
11	5.387	VV	0.1604	41.95073	3.87322	0.8369
12	6.075	VB	0.2580	89.54916	5.32926	1.7864
13	9.558	BB	0.2623	56.30305	3.18405	1.1232
14	10.229	BB	0.2053	17.19465	1.25928	0.3430
Totals :				5012.71680	524.89493	

Signal 3: DAD1 E, Sig=280,16 Ref=off

Peak #	RetTime [min]	Type	Width [min]	Area [mAU*s]	Height [mAU]	Area %
1	1.499	BV	0.1286	10.58568	1.25229	1.1527
2	1.661	VV	0.0985	36.74335	5.32257	4.0011
3	2.052	VV	0.1664	18.03585	1.49839	1.9640
4	2.194	VB	0.0995	21.44307	3.07095	2.3350
5	2.805	VB	0.1071	24.55502	3.53312	2.6739
6	3.399	BV	0.1386	19.37074	2.11923	2.1094
7	3.669	VB	0.1405	771.93689	81.47997	84.0591
8	6.080	BB	0.1978	15.65542	1.15759	1.7048
Totals :				918.32603	99.43412	

Signal 4: DAD1 G, Sig=300,16 Ref=off

Peak #	RetTime [min]	Type	Width [min]	Area [mAU*s]	Height [mAU]	Area %
1	1.661	BB	0.0938	35.94694	5.53011	10.2711
2	2.050	BV	0.1183	9.72066	1.22862	2.7775
3	2.194	VB	0.0947	20.68534	3.14590	5.9104
4	2.804	BB	0.1052	7.19315	1.06024	2.0553
5	3.392	BV	0.1388	9.41847	1.02932	2.6911
6	3.669	VB	0.1405	267.01852	28.18267	76.2947
Totals :				349.98308	40.17687	

Data File C:\Chem32\1\Data\Jake\ABS-I-99.D
Sample Name: ABS-I-99

Signal 5: DAD1 H, Sig=320,16 Ref=off

Peak #	RetTime [min]	Type	Width [min]	Area [mAU*s]	Height [mAU]	Area %
1	1.662	BB	0.0778	6.56233	1.27988	10.3584
2	2.195	VB	0.0963	12.99295	1.93521	20.5088
3	3.669	BB	0.1366	43.79768	4.79417	69.1328
Totals :				63.35296	8.00926	

*** End of Report ***

REFERENCES

(1) What Is Cancer? https://www.cancer.gov/about-cancer/understanding/what-is-cancer (accessed Feb 17, 2020).

(2) What Is Cancer? https://www.cancer.org/cancer/cancer-basics/what-is-cancer.html (accessed Feb 17, 2020).

(3) Siemann, D. W. The Unique Characteristics of Tumor Vasculature and Preclinical Evidence for Its Selective Disruption by Tumor-Vascular Disrupting Agents. *Cancer Treatment Reviews* **2011**, *37* (1), 63–74. https://doi.org/10.1016/j.ctrv.2010.05.001.

(4) Mason, R. P.; Zhao, D.; Liu, L.; Trawick, M. L.; Pinney, K. G. A Perspective on Vascular Disrupting Agents That Interact with Tubulin: Preclinical Tumor Imaging and Biological Assessment. *Integr Biol (Camb)* **2011**, *3* (4), 375–387. https://doi.org/10.1039/c0ib00135j.

(5) Gillian M. Tozer; Chryso Kanthou; Bruce C. Baguley. Disrupting Tumour Blood Vessels. *Nature Reviews Cancer* **2005**, *5* (6), 423–435. https://doi.org/10.1038/nrc1628.

(6) Cocco, G.; Chu, D. C. C.; Pandolfi, S. Colchicine in Clinical Medicine. A Guide for Internists. *European Journal of Internal Medicine* **2010**, *21* (6), 503–508. https://doi.org/10.1016/j.ejim.2010.09.010.

(7) Cragg, G. M.; Newman, D. J. Plants as a Source of Anti-Cancer Agents. *Journal of Ethnopharmacology* **2005**, *100* (1–2), 72–79. https://doi.org/10.1016/j.jep.2005.05.011.

(8) Tron, G. C.; Pirali, T.; Sorba, G.; Pagliai, F.; Busacca, S.; Genazzani, A. A. Medicinal Chemistry of Combretastatin A4: Present and Future Directions. *Journal of medicinal chemistry* **2006**, *49* (11), 3033–3044. https://doi.org/10.1021/jm0512903.

(9) Liu, L.; Trawick, M. L.; Pinney, K.; Mason, R. P. Abstract 4194: Assessment of Novel Benzosuberene-Based Vascular Disrupting Agents (VDA) on Diverse Tumor Lines. *Cancer Res* **2016**, *76* (14 Supplement), 4194–4194. https://doi.org/10.1158/1538-7445.AM2016-4194.

(10) Tanpure, R. P.; George, C. S.; Strecker, T. E.; Devkota, L.; Tidmore, J. K.; Lin, C.-M.; Herdman, C. A.; MacDonough, M. T.; Sriram, M.; Chaplin, D. J.; et al.

Synthesis of Structurally Diverse Benzosuberene Analogues and Their Biological Evaluation as Anti-Cancer Agents. *Bioorganic & Medicinal Chemistry* **2013**, *21* (24), 8019–8032. https://doi.org/10.1016/j.bmc.2013.08.035.

(11) Nogales, E.; Wolf, S. G.; Downing, K. H. Structure of the Alpha-Beta Tubulin Dimer by Electron Crystallography. *Nature* **1998**, *391* (2), 199.

(12) Niu, H.; Strecker, T. E.; Gerberich, J. L.; Campbell, J. W.; Saha, D.; Mondal, D.; Hamel, E.; Chaplin, D. J.; Mason, R. P.; Trawick, M. L.; et al. Structure Guided Design, Synthesis, and Biological Evaluation of Novel Benzosuberene Analogues as Inhibitors of Tubulin Polymerization. *Journal of medicinal chemistry* **2019**, *62* (11), 5594–5615. https://doi.org/10.1021/acs.jmedchem.9b00551.

(13) Devkota, L.; Lin, C.-M.; Strecker, T. E.; Wang, Y.; Tidmore, J. K.; Chen, Z.; Guddneppanavar, R.; Jelinek, C. J.; Lopez, R.; Liu, L.; et al. Design, Synthesis, and Biological Evaluation of Water-Soluble Amino Acid Prodrug Conjugates Derived from Combretastatin, Dihydronaphthalene, and Benzosuberene-Based Parent Vascular Disrupting Agents. *Bioorganic & Medicinal Chemistry* **2016**, *24* (5), 938–956. https://doi.org/10.1016/j.bmc.2016.01.007.

(14) Tanpure, R. P.; George, C. S.; Sriram, M.; Strecker, T. E.; Tidmore, J. K.; Hamel, E.; Charlton-Sevcik, A. K.; Chaplin, D. J.; Trawick, M. L.; Pinney, K. G. An Amino-Benzosuberene Analogue That Inhibits Tubulin Assembly and Demonstrates Remarkable Cytotoxicity. *Medchemcomm* **2012**, *3* (6), 720–724. https://doi.org/10.1039/C2MD00318J.

(15) Structural interrogation of benzosuberene-based inhibitors of tubulin polymerization - ScienceDirect https://www-sciencedirect-com.ezproxy.baylor.edu/science/article/pii/S0968089615300900 (accessed Apr 20, 2020).

(16) Pinney, K.; Mocharla, V.; Chen, Z.; Garner, C.; Ghatak, A.; Hadimani, M.; Kessler, J.; Dorsey, J.; Edvardson, K.; Chaplin, D.; et al. TUBULIN BINDING AGENTS AND CORRESPONDING PRODRUG CONSTRUCTS. 12.

(17) Pinney, K. G.; Sriram, M.; George, C.; Tanpure, R. P. Efficient Method for Preparing Functionalized Benzosuberenes. WO2012068284A2, May 24, 2012.

(18) Mondal, D.; Ford, J.; Pinney, K. G. Improved Methodology for the Synthesis of a Cathepsin B Cleavable Dipeptide Linker, Widely Used in Antibody-Drug Conjugate Research. *Tetrahedron Letters* **2018**, *59* (40), 3594–3599. https://doi.org/10.1016/j.tetlet.2018.08.021.

(19) Lambert, J. M. Antibody–Drug Conjugates (ADCs): Magic Bullets at Last! *Mol. Pharmaceutics* **2015**, *12* (6), 1701–1702. https://doi.org/10.1021/acs.molpharmaceut.5b00302.

(20) Senter, P. D.; Sievers, E. L. The Discovery and Development of Brentuximab Vedotin for Use in Relapsed Hodgkin Lymphoma and Systemic Anaplastic Large Cell Lymphoma. *Nature Biotechnology; New York* **2012**, *30* (7), 631–637. http://dx.doi.org/10.1038/nbt.2289.

(21) Perez, H. L.; Cardarelli, P. M.; Deshpande, S.; Gangwar, S.; Schroeder, G. M.; Vite, G. D.; Borzilleri, R. M. Antibody–Drug Conjugates: Current Status and Future Directions. *Drug Discovery Today* **2014**, *19* (7), 869–881. https://doi.org/10.1016/j.drudis.2013.11.004.

(22) Mondal, D.; Niu, H.; Pinney, K. G. Efficient Synthetic Methodology for the Construction of Dihydronaphthalene and Benzosuberene Molecular Frameworks. *Tetrahedron Lett* **2019**, *60* (5), 397–401. https://doi.org/10.1016/j.tetlet.2018.12.033.

(23) Lei, X.; Chen, M.; Li, X.; Huang, M.; Nie, Q.; Ma, N.; Chen, H.; Xu, N.; Ye, W.; Zhang, D. A Vascular Disrupting Agent Overcomes Tumor Multidrug Resistance by Skewing Macrophage Polarity toward the M1 Phenotype. *Cancer Letters* **2018**, *418*, 239–249. https://doi.org/10.1016/j.canlet.2018.01.016.

(24) Boucher, Y.; Baxter, L. T.; Jain, R. K. Interstitial Pressure Gradients in Tissue-Isolated and Subcutaneous Tumors: Implications for Therapy. *Cancer research* **1990**, *50* (15), 4478–4484.

(25) Tozer, G. M.; Prise, V. E.; Wilson, J.; Locke, R. J.; Vojnovic, B.; Stratford, M. R.; Dennis, M. F.; Chaplin, D. J. Combretastatin A-4 Phosphate as a Tumor Vascular-Targeting Agent: Early Effects in Tumors and Normal Tissues. *Cancer research* **1999**, *59* (7), 1626–1634.

(26) Jain, R.; Baxter, L. Mechanisms of Heterogeneous Distribution of Monoclonal Antibodies and Other Macromolecules in Tumors: Significance of Elevated Interstitial Pressure. *Cancer Research* **1988**, *48* (24 Pt 1), 7022–7032.

(27) Anonymous. Mylotarg. *Formulary* **2000**, *35* (7), 553.

(28) Bornstein, G. G. Antibody Drug Conjugates: Preclinical Considerations. *AAPS J* **2015**, *17* (3), 525–534. https://doi.org/10.1208/s12248-015-9738-4.

(29) Kovtun, Y. V.; Audette, C. A.; Mayo, M. F.; Jones, G. E.; Doherty, H.; Maloney, E. K.; Erickson, H. K.; Sun, X.; Wilhelm, S.; Ab, O.; et al. Antibody-Maytansinoid Conjugates Designed to Bypass Multidrug Resistance. *Cancer Res* **2010**, *70* (6), 2528–2537. https://doi.org/10.1158/0008-5472.CAN-09-3546.

(30) Dubowchik, G. M.; Firestone, R. A.; Padilla, L.; Willner, D.; Hofstead, S. J.; Mosure, K.; Knipe, J. O.; Lasch, S. J.; Trail, P. A. Cathepsin B-Labile Dipeptide

Linkers for Lysosomal Release of Doxorubicin from Internalizing Immunoconjugates: Model Studies of Enzymatic Drug Release and Antigen-Specific In Vitro Anticancer Activity. *Bioconjugate Chem.* **2002**, *13* (4), 855–869. https://doi.org/10.1021/bc025536j.

(31) Improved Methodology for the Synthesis of a Cathepsin B Cleavable Dipeptide Linker, Widely Used in Antibody-Drug Conjugate Research - ScienceDirect https://www-sciencedirect-com.ezproxy.baylor.edu/science/article/pii/S0040403918310025?via%3Dihub (accessed Mar 18, 2020).

(32) Gébleux, R.; Stringhini, M.; Casanova, R.; Soltermann, A.; Neri, D. Non-Internalizing Antibody–Drug Conjugates Display Potent Anti-Cancer Activity upon Proteolytic Release of Monomethyl Auristatin E in the Subendothelial Extracellular Matrix. *International Journal of Cancer* **2017**, *140* (7), 1670–1679. https://doi.org/10.1002/ijc.30569.

(33) Polson, A. G.; Calemine-Fenaux, J.; Chan, P.; Chang, W.; Christensen, E.; Clark, S.; de Sauvage, F. J.; Eaton, D.; Elkins, K.; Elliott, J. M.; et al. Antibody-Drug Conjugates for the Treatment of Non-Hodgkin's Lymphoma: Target and Linker-Drug Selection. *Cancer Research* **2009**, *69* (6), 2358–2364. https://doi.org/10.1158/0008-5472.CAN-08-2250.

(34) Matsumura, Y. Cancer Stromal Targeting (CAST) Therapy. *Advanced Drug Delivery Reviews* **2012**, *64* (8), 710–719. https://doi.org/10.1016/j.addr.2011.12.010.

(35) Bosslet, K.; Straub, R.; Blumrich, M.; Czech, J.; Gerken, M.; Sperker, B.; Kroemer, H. K.; Gesson, J.-P.; Koch, M.; Monneret, C. Elucidation of the Mechanism Enabling Tumor Selective Prodrug Monotherapy. *Cancer Res* **1998**, *58* (6), 1195–1201.

(36) Dan, N.; Setua, S.; Kashyap, V. K.; Khan, S.; Jaggi, M.; Yallapu, M. M.; Chauhan, S. C. Antibody-Drug Conjugates for Cancer Therapy: Chemistry to Clinical Implications. *Pharmaceuticals (Basel)* **2018**, *11* (2). https://doi.org/10.3390/ph11020032.

(37) Beck, A.; Goetsch, L.; Dumontet, C.; Corvaïa, N. Strategies and Challenges for the next Generation of Antibody–Drug Conjugates. *Nature Reviews Drug Discovery* **2017**, *16* (5), 315–337. https://doi.org/10.1038/nrd.2016.268.

(38) Doronina, S. O.; Mendelsohn, B. A.; Bovee, T. D.; Cerveny, C. G.; Alley, S. C.; Meyer, D. L.; Oflazoglu, E.; Toki, B. E.; Sanderson, R. J.; Zabinski, R. F.; et al. Enhanced Activity of Monomethylauristatin F through Monoclonal Antibody Delivery: Effects of Linker Technology on Efficacy and Toxicity. *Bioconjugate Chem.* **2006**, *17* (1), 114–124. https://doi.org/10.1021/bc0502917.

(39) Anti-Cancer ADC Drugs: 3 Design Elements, 7 Approved ADCs, Multiple Clinical Trials | Biochempeg https://www.biochempeg.com/article/74.html (accessed Apr 8, 2020).

(40) Polivy FDA Report. https://www.accessdata.fda.gov/drugsatfda_docs/label/2019/761121s000lbl.pdf.

(41) Padcev™ FDA Report. https://www.accessdata.fda.gov/drugsatfda_docs/label/2019/761137s000lbl.pdf.

(42) MYLOTARGTM (Gemtuzumab Ozogamicin) for Injection. 19. https://www.accessdata.fda.gov/drugsatfda_docs/label/2017/761060lbl.pdf.

(43) Besponsa™ FDA Report. https://www.accessdata.fda.gov/drugsatfda_docs/label/2017/761040s000lbl.pdf.

(44) Trastuzumab Deruxtecan (Enhertu™) FDA Report. https://www.accessdata.fda.gov/drugsatfda_docs/label/2019/761139s000lbl.pdf.

(45) Kadcyla FDA Report. https://www.accessdata.fda.gov/drugsatfda_docs/label/2019/125427s105lbl.pdf.

(46) Chattopadhyay, N.; Syed, S.; Zhang, Y.; Yu, J.; He McDougall, D.; Yu, L. Y.; Tirrell, S.; Berger, A.; van de Velde, H.; Tremblay, C.; et al. Ninlaro (Ixazomib) and Brentuximab Vedotin (ADCETRIS) Combination Results in Synergistic Antitumor Activity in Mouse Models of CD30 Positive Anaplastic Large Cell Lymphoma. *Blood* **2016**, *128* (22), 1842–1842. https://doi.org/10.1182/blood.V128.22.1842.1842.

(47) Chakravarty, P. K.; Carl, P. L.; Weber, M. J.; Katzenellenbogen, J. A. Plasmin-Activated Prodrugs for Cancer Chemotherapy. 1. Synthesis and Biological Activity of Peptidylacivicin and Peptidylphenylenediamine Mustard. *J. Med. Chem.* **1983**, *26* (5), 633–638. https://doi.org/10.1021/jm00359a003.

(48) Pinney, K.; Lin, C.; Mondal, D.; Ford, J. Drug-Linker Conjugate Pharmaceutical Compositions, April 20, 2017.

(49) Pochopin, N. L.; Charman, W. N.; Stella, V. J. Amino Acid Derivatives of Dapsone as Water-Soluble Prodrugs. *International Journal of Pharmaceutics* **1995**, *121* (2), 157–167. https://doi.org/10.1016/0378-5173(95)00005-4.

(50) Vig, B. S.; Huttunen, K. M.; Laine, K.; Rautio, J. Amino Acids as Promoieties in Prodrug Design and Development. *Advanced Drug Delivery Reviews* **2013**, *65* (10), 1370–1385. https://doi.org/10.1016/j.addr.2012.10.001.

(51) Ohsumi, K.; Hatanaka, T.; Nakagawa, R.; Fukuda, Y.; Morinaga, Y.; Suga, Y.; Nihei, Y.; Ohishi, K.; Akiyama, Y.; Tsuji, T. Synthesis and Antitumor Activities of Amino Acid Prodrugs of Amino-Combretastatins. *Anti-Cancer Drug Design* **1999**, *14* (6), 539–548.

(52) Kern, J. C.; Dooney, D.; Zhang, R.; Liang, L.; Brandish, P. E.; Cheng, M.; Feng, G.; Beck, A.; Bresson, D.; Firdos, J.; et al. Novel Phosphate Modified Cathepsin B Linkers: Improving Aqueous Solubility and Enhancing Payload Scope of ADCs. *Bioconjugate Chem.* **2016**, *27* (9), 2081–2088. https://doi.org/10.1021/acs.bioconjchem.6b00337.